EUROPEAN ORGANISATION FOR NUCLEAR RESEARCH

CERN/DRDC/93-49
RD5 / Status Report
January 5, 1994

Status Report of the RD5 Experiment

H. Faissner, T. Moers, R. Priem, B. Razen, D. Rein, H. Reithler, H.Schwarthoff, H. Tuchscherer, H. Teykal and H. Wagner
III. Physikalisches Institut A, RWTH Aachen, Germany

F. Bakker, G. Brouwer, A-P. Colijn, W. Gotink, H. Groenstege, P. Rewiersma, S. Sman, H. Tolsma, G. van Apeldoorn, J. van Eldik, and H. van der Graaf
NIKHEF-H, Amsterdam, The Netherlands

J. Shank and S. Whitaker
Boston University, USA

V. Gratchev[1)], V. Polychronakos, V. Tcherniatine[2)], A. Vanyashin[2)]
Brookhaven National Laboratory, USA

Gy. L. Bencze, E. Denes, A. Ster, L. Urban and G. Vesztergombi
Central Research Inst. for Physics, KFKI, Budapest, Hungary

J. L. Bénichou, M. Della Negra*), A. Hervé, S. Inkinen[3)], J.-M. Le Goff, A. Onnela[4)], D. Peach, J. Pothier, B. Powell, E. Radermacher*), R. Ribeiro, C. Seez [5)], G. Waurick and G. Wrochna[6)]
CERN, Geneva, Switzerland

A. Bizzeti, C. Civinini, R. D'Alessandro, M. Meschini and V. Pojidaev
University of Firenze and INFN Sezione di Firenze, Italy

R. Kinnunen and J. Tuominiemi
Laboratory for High Energy Physics, Department of Physics, University of Helsinki, Finland

S. Czellar, M. Hakovirta, M. Huhtinen, M. Juntunen, V. Karimäki, R. Lauhakangas, R. Orava, E. Pietarinen, M. Pimiä, J. P. Saarikko, T. Tuuva and M. Voutilainen
Research Institute for High Energy Physics, SEFT, University of Helsinki, Finland

D. Cline, D. Chrisman, S. Lazic and S. Otwinowski
University of California, Los Angeles, USA

C. Lyndon and R. McNeil
Louisiana State University, USA

A. Ferrando, M. C. Fouz, A. Iglesias, M. I. Josa, L. Martinez-Laso and J. M. Salicio
CIEMAT, Madrid, Spain

C. Albajar
Universitad Autónoma, Madrid, Spain

A. Arefiev, E. Choumilov, Yu. Galaktionov, Yu. Kolotaev, A. Malinin, V. Plyaskin and A. Rojkov
Institute for Theoretical and Experimental Physics (ITEP), Moskva, USSR

R. Bergman, C. Brouwer, A. C. König, C. L. A. Pols and T. Wijnen
University of Nijmegen and NIKHEF, The Netherlands

A. Bettini, P. Casoli, S. Centro, F. Gasparini, R. Martinelli, A. Meneguzzo, P. Sartori and P. Zotto[7)]
Dipartimento di Fisica, Università di Padova, Italy

P. Giacomelli, W. Gorn, J. G. Layter, B. C. Shen and G. W. Wilson
University of California, Riverside, USA

C. Bacci[8)], F. Ceradini[8)], G. Ciapetti, F. Lacava, A. Nisati, D. Orestano, E. Petrolo, L. Pontecorvo, A. Tusi, S. Veneziano, M. Verzocchi and L. Zanello
Dipartimento di Fisica, Università di Roma "La Sapienza" and INFN, Italy

R. Cardarelli, A. Di Ciaccio and R. Santonico
Dipartimento di Fisica, Università di Roma "Tor Vergata" and INFN, Italy

M. Mohammadi and A. Sanjari
State University of New York at Stony Brook, USA

K. Österberg
Physics Department, Åbo Akademi, Turku, Finland

M. Andlinger, A. Kluge, B. Koch, R. Labner, P. Porth, N. Sinanis, F. Szoncso, G. Walzel and C.-E. Wulz
HEPHY, Österreichische Akademie der Wissenschaften, Vienna, Austria

H. Czyrkowski, W. Dominik, I. Kudla, M. Konecki, J. Królikowski, M. Lewandowski and L. Ropelewski
Institute of Experimental Physics, Warsaw University, Poland

M. Górski and M. Szeptycka
Institute for Nuclear Studies, Warsaw, Poland

P. Le Coultre
Institut für Hochenergiephysik, Eidgenössische Technische Hochschule, Zürich, Switzerland

*) Joint spokesmen
1) Visitor from Saint-Petersburg Nuclear Physics Institute, Gatchina, Russia
2) Visitor from Moscow Engineering Physics Institute, Russia
3) Visitor from Research Institute for High Energy Physics, SEFT, Helsinki University, Helsinki, Finland
4) Visitor from Helsinki University of Technology, Helsinki, Finland
5) Visitor from Imperial College, London, UK
6) Visitor from Institute of Experimental Physics, Warsaw University, Poland
7) Now at Dip. di Fisica del Politecnico di Milano and Sezione dell'INFN di Padova, Italy
8) Now at Dipartimento di Fisica "E.Amaldi", III Universita' di Roma, Italy

Contents

Acknowledgments

The unfailing help of P. Pétiot is kindly acknowledged.

The authors also acknowledge the support of the following funding agencies:

- Deutsches Bundesministerium für Forschung und Technologie,
- Hungarian Academy of Science under grant OTKA-4089,
- Spanish CICYT under grants AEN92-0829 and AEN-93-0954-E,
- Instituto Nazionale di Fisica Nucleare, Italy,
- Texas National Research Laboratory Commission – award numbers RGFY92-118 and RGFY93-312A,
- US Department of Energy – contract numbers DE-AC02-76CH00016, DE-FG05-91ER40617 and DE-FG02-92ER40697,
- Polish Committee for Scientific Research under grants KBN-PB-2 0422 91 01 and KBN-SPUB-206/93.

1 Introduction

The RD5 program covers several topics related to muon detection at LHC: punchthrough measurements, trigger studies, muon momentum measurements, and tests of various types of large area muon chambers [1]. Since 1991 about 10^7 muon and hadron events were recorded during 15 weeks of running time and several results have already been published [2]–[7]. In this status report we present a summary of the results obtained in the last two years and conclude with the program foreseen for 1994.

In section 2 we review the RD5 detector in its present form including a description of modifications and detector additions since 1991.

Since 1992 the superconducting 3T EHS magnet [8] was operational and punchthrough probabilities were obtained as a function of magnetic field, absorber depth and of incident hadron momentum. In addition, the momentum and angular distributions of punchthrough particles for different incident hadron momenta based on track measurements in the muon stations were analyzed. Studies of effects due to muon induced electromagnetic showers affecting chamber performances have been made. All these results are summarized in section 3.

First results on trigger efficiencies as a function of the muon momentum are presented in section 4 for a trigger based on Resistive Plate Chambers (RPCs) in front, inside and after 1.8 m of magnetized iron.

Finally we report in section 5 on the performance of different types of muon chambers which are candidates in an LHC experiment either for the muon trigger, like RPCs and Parallel Plate Chambers (PPCs), or for precise muon track measurement, like Honeycomb Strip Chambers (HSCs), Drift Chambers with Bunch Crossing Capability (DTBXs), Wall-Less Drift Chambers (WLDCs) or Cathode Strip Chambers (CSCs).

In 1994 it is planned to pursue the tests on muon trigger processors and the optimization of large muon chamber prototypes.

2 Detector Description

The RD5 experiment is situated on the H2 beam of the SPS North Area. The experimental setup is shown in Fig. 1. It consists of two magnets, a superconducting solenoid having a 3 Tesla field (the old EHS magnet referred to as M1) and an absorber magnet (M2) having a 1.5 Tesla field. This setup can simulate a solenoidal detector with its return yoke, and, switching off the M1, a toroidal spectrometer for possible experiments at LHC. The beam definition is given by two multiwire proportional chambers (MWPCs: U1 and U3) and a silicon beam telescope (SiBT). The scintitillator counters are used by the trigger system. The tracking calorimeter (TRACAL) serves as a calorimeter/absorber. Three muon stations are installed in front of, inside and behind the absorber magnet. The muon drift chambers (taken from UA1 experiment) are used for precise measurement of the trajectories in the RD5 spectrometer. The RPCs are part of the muon measurement system and used also for triggering purposes. The present RD5 setup is basically the same as that presented in 1991 [2], however, different modifications have been made in order to improve the detector and adapt it to new tasks. Apart from the M1 magnet which started to operate from 1992, the trigger system, the beam definition, TRACAL, RPC hodoscope and the Data Acquisition System (DAS) have been improved or completed as described in Sec. 2.1-2.6. In addition, various chamber prototypes have been installed for tests (see Sec. 5).

2.1 Magnets

The M1 magnet was previously used in the NA36 experiment. A series of measurements has shown that the field map existing from NA36 [9] is still valid (at least between the coils) despite the two big iron blocks (the M2 and the iron mirror) which were installed after the field map had been made. The old field map was prepared for a current of 3600 A while we operate M1 up to 4000 A, therefore a scale factor must be applied to the field map to account for the different currents.

There exists a calculated field map for the M2 magnet as well [10]. Our first trial to measure the field indicates that the field is lower than was expected from the calculations. It was suspected that this difference was due to a mutual interference between the two magnets. Investigation of this hypothesis must await a different measurement method then previously used.

2.2 Trigger

The RD5 trigger system has been significantly updated since 1991. The most important modifications were the installation of a 4×4 m^2 RPC wall for the VETO system (see also Sec. 2.5) and the utilisation of RPCs for muon triggers. The trigger system in its present form (see also Fig. 1) consists of scintillators S1 and S5 for the beam definition and S4a-b for beam size determination. The system of counters S2 and S3 together with the RPC wall form a VETO system against beam halo particles. It is ensured that there are no other particles crossing the 4×4 m^2 area within $\pm 2\mu$s around the triggering one. Part of the 2×2 m^2 RPCs in the muon stations 1 and 2 provide muon triggers after 10λ and 20λ for punchthrough study. A system of scintillation counters S7 behind the M2 (30λ) covering 100×250 cm^2 area helps in off-line muon identification. A Cerenkhov counter CEDAR, being a standard H2 beam equipment, is used for running with positive pions, kaons and protons in order to distinguish various kinds of particles.

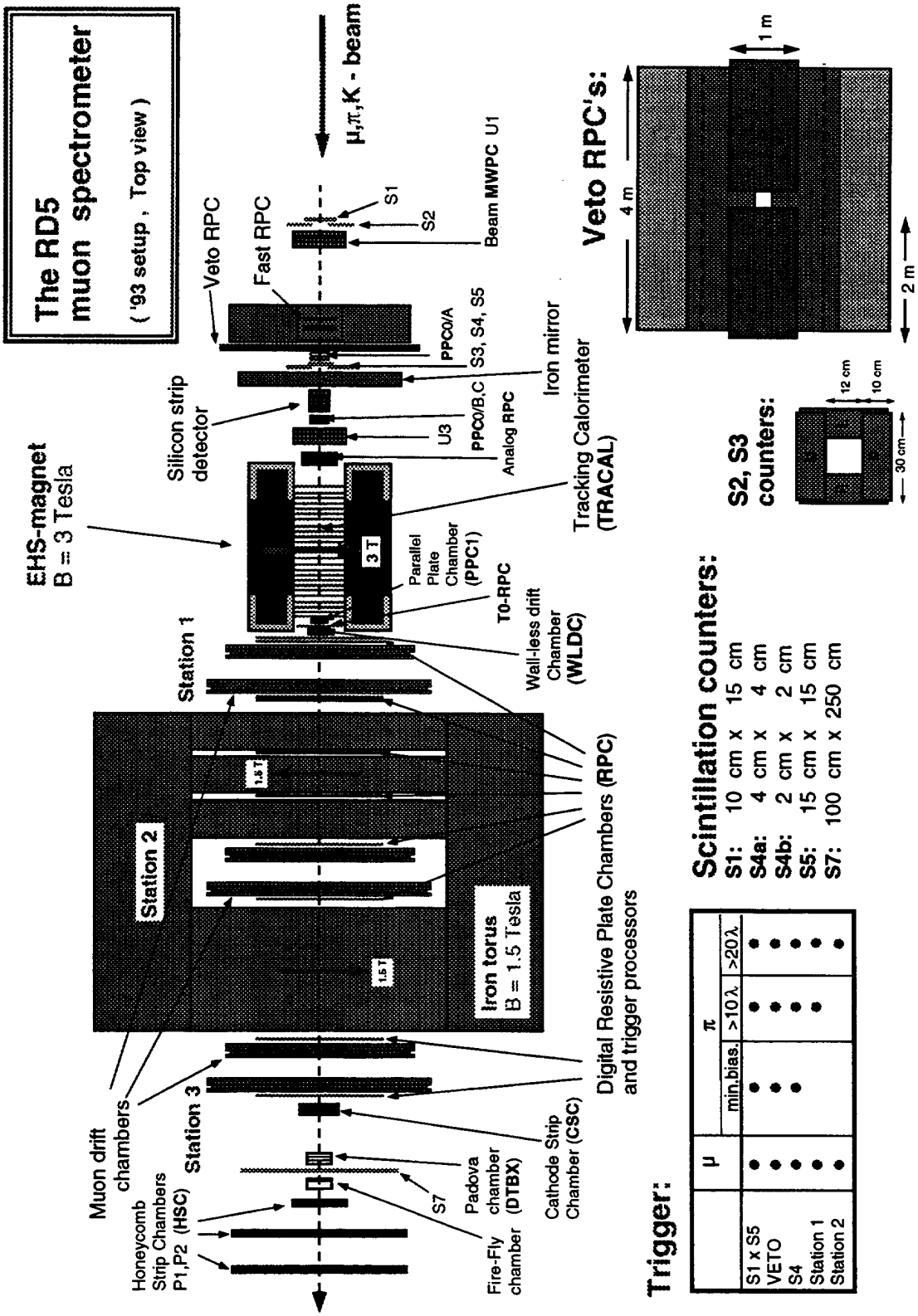

Figure 1: Schematic of the RD5 detector it its 1993 configuration.

In addition to the general purpose facilities described above the RD5 trigger contains some devices for dedicated studies of various detector prototypes. There is an additional upstream scintillation counter for the PPC Very Forward Calorimeter prototype, two downstream scintillators for the Cathode Strip Chamber and a few PPC chambers of 2×2 cm^2 for a PPC test program.

More details on the RD5 trigger system are given in a technical note [11].

2.3 Beam definition

During the 1991-1992 runs the beam defining MWPCs showed some weak points: gas leakage, dead areas, poor efficiency, and instability (this latter mainly due to the gas mixture used). For 1993 one of the chambers (U3) was replaced by a repaired spare one and a new gas mixture (argon-39%, isobutane-24%, carbon dioxide-37%) was used at 5.1 kV. The chambers now work perfectly but a new readout system must be implemented in the near future. The third MWPC (W2) was very unstable and had to be remowed after 1991.

The SiBT was put immediately behind the iron mirror to make the electromagnetic shower study possible. In 1991 the SiBT readout system was independent from RD5, now it is integrated into the RD5 DAS.

2.4 TRACAL

The principle of the TRACAL is described in reference [4]. In 1991 only the central 48 strips of each of the single-layer HSCs were equipped with readout electronics. The upgrade before the 1992 experimental periods invoked the increase of the number of strip channels to be read out. The air cooling of the strip readout electronics was improved to avoid problems which might occur due to the extra heat dissipation. Moreover, the low voltage distribution for both strip and wire preamplifiers was improved.

Several other items were improved with respect to the 1991 setup. The flat twisted pair cables used for the wire readout were replaced by shielded twisted pair cables to reduce the effect of cross-talk. Furthermore, each single-layer HSC obtained its own individual gas input (Ar/CO_2 mixture) instead of having two single-layers connected in parallel to a single gas line. Detection inefficiencies due to a wrong gas mixture related to a bad gas flow were hereby solved.

Normally a honeycomb structure has an intrinsic mechanical stiffness. However, in the geometry used for the HSCs in TRACAL (single-layer), it was noticed that some layers were bent. This bending had the consequence that the anode wire was not positioned properly in the center of the hexagonal tube. Hence, high voltage breakdowns occurred quite often. Rigid aluminum plates with a thickness of 2 mm were mounted on the single-layer HSCs to straighten them and to overcome the problem of the HV breakdowns. Finally, the two independent TRACAL units inside of M1 were tilted at an angle of 0.1 rad around an axis parallel to the strips to compensate for the Lorentz angle.

2.5 Resistive Plate Chambers (RPC)

The RPC hodoscope has been modified in two steps since the first RD5 run in 1991. The analysis of the '91 data has shown that, for the study of the probability of punchthrough of hadronic showers at various depths in the detector, there was need for an efficient veto against hits produced by off-time and halo particles. A veto counter that covers the area of the drift chambers was built with an array of RPCs placed 1.2 m upstream of the M1 magnet. The array (Fig. 1) has a rectangular hole of variable size in the center to allow the beam to pass through. The signal, obtained by OR-ing the fast signals from all strips, is used for a Veto by the trigger system.

Four new 2×2 m^2 planes of RPC were added in the second and in the third muon measurement station with one plane on either side of the drift chambers. Each plane is made of two RPCs with read-out strips that measure the coordinate in the bending plane. They are used to extend the measurement of punchthrough and the fast tracking of muons at large depths.

All new detector planes are made of double-gap RPCs that insure a better efficiency and a more precise timing. These RPCs were manufactured and assembled by industry, delivered at CERN and tested only after installation: all of them worked properly. More details on the construction and the performance of the double-gap RPC are given in Sec. 5.1.

2.6 Data Acquisition System (DAS)

The RD5 data acquisition system has been continuously developed since the start of RD5. In its present configuration, the system is built with modular blocks each of which is a VME-crate with at least one CPU. The VSB standard is used as a high speed crate interconnect. Data come from various other standards such as CAMAC, REMUS, FastBus, RMH, VME custom built modules, optical fibres, SPS-serial link, TransPuters. All of them are interfaced into VME using dedicated low-cost CPU's. In RD5, including some recent upgrades, 12 VME-crates form what we call the frontend. Two further VME crates serve as the system's star point and as the final readout buffer. Local monitoring, high voltage control and network access reside in three more VME-crates. Data passes through one of the frontends, a set of dual port memories common to each system star point and frontend, the event builder, the ZEBRA-formatter and finally onto IBM-compatible cassettes of 200 Mb each. System development, control and monitoring is mainly done via three MacIntosh IIfx computers. The recent addition of a SUN workstation enables remote access to the data acquisition that so far has been running without

any network connection. Further upgrades of the RD5 data acquisition are not foreseen as the system performance (and flexibility) is well matched to the requirements. Addition of new detectors is a matter of hours. The readout time is typically 6 ms for an average size event, the main limitation being the extensive use of CAMAC-modules (more than 2000 channels). However steps have been taken to devise a prototype LHC-like data acquisition using the existing setup as the starting point. System flexibility as well as performance will have to gradually approach higher data rates, pipeline control and a control structure that will not any more exhibit the traditional spill cycle.

3 Physics Program

The RD5 physics program involves the study of phenomena that affect the muon detection in LHC experiments.

Punchthrough of hadronic showers, including the total probability and the momentum and angular spectrum of punchthrough particles have been measured and the results are used for checking and tuning Monte Carlo programs simulating future LHC detectors.

Electromagnetic secondaries induced by muons were studied using the SiBT and different muon chambers such as HSC (TRACAL), WLDC and DTBX.

3.1 Total punchthrough

We define the total punchthrough probability of hadronic showers at a given depth x as the ratio of the number of events with at least one hit in the detector at that depth x over the total number of events. An algorithm, which accounts for chamber efficiencies and noise levels, was developed in order to find the actual penetration depth of each punchthrough particle [3].

In 1991 first punchthrough data were taken with negative muon and pion beams. The beam momenta were 30, 40, 50, 75, 100, 200 and 300 GeV/c. The muon data were used to characterize the muon contamination in the pion beam and for detector calibration. The results of the analysis of 1991 data, including a detailed description of the analysis methods used, have been previously published [2, 3]. In 1992 and 1993 the RD5 data set was expanded to include negative pions of 10 and 20 GeV/c as well as positive hadrons (π^+, K^+ and protons) of 30–300 GeV/c. Data were also taken with the M1 magnet at full field (3 Tesla) and at half field.

In Figure 2 we show the punchthrough probability of 10 and 20 GeV/c negative pions as a function of meters of equivalent iron. The punchthrough probability of the 10 GeV/c pions was only measured up to 2.9 m Fe equivalent. This is because of difficulties in subtracting the primary muon background. We regard as muons those events having one minimum ionizing track in TRACAL and a penetration depth up to Station 3 (see reference [3] for details). For a large number of muons in the 10 GeV/c pion beam, this definition fails because many of these muons are bent by the absorber magnet outside the acceptance of Station 3. Therefore, no hit is recorded in Station 3 and, as a result, the particle appears to have stopped between Station 2 and Station 3. Alternate methods for subtracting the muon contamination from 10 GeV/c data are being investigated.

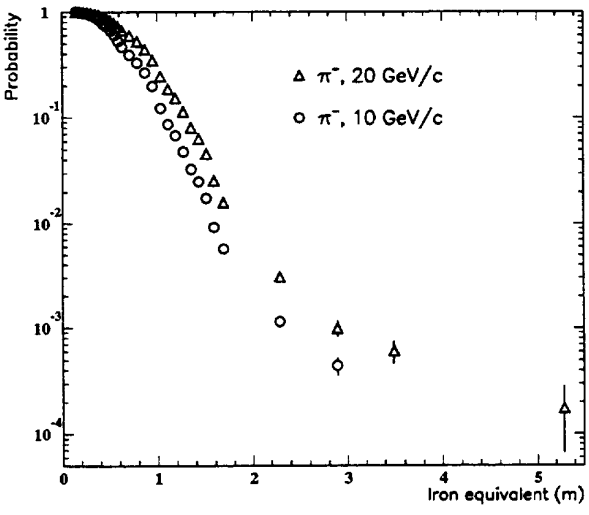

Figure 2: Punchthrough probability as a function of meters of equivalent iron for 10 GeV/c and 20 GeV/c π^-.

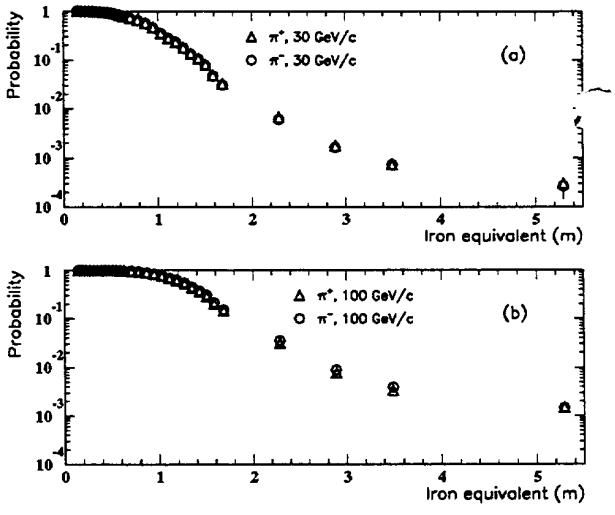

Figure 3: Punchthrough probability as a function of meters of equivalent iron for a) 30 GeV/c π^+ and π^- and b) 100 GeV/c π^+ and π^-.

Punchthrough results with positive particles are presented in Figure 3. We present a comparison between 30 GeV/c π^+ and π^- (Fig. 3a) and 100 GeV/c π^+ and π^- (Fig. 3b). There appears to be no significant difference in the punchthrough probability of positive and negative pions.

The effect of the magnetic field of M1 on the punchthrough probability is presented in Figure 4. These results should be considered as only preliminary. In order to publish meaningful results concerning the effect of the M1 magnet on punchthrough, a Monte Carlo study of the acceptance of the RD5 detector must be completed. With the M1 magnet turned on, the punchthrough particles, which in general have a low momentum, exit the magnet at large angles with respect to the beam line and are deflected outside the acceptance of the detector. The losses due to this magnet bending must be corrected for.

The punchthrough probability at Station 1 (10λ), Station 2 (21λ) and Station 3 (32λ) as a function of initial pion momentum is presented in Figure 5.

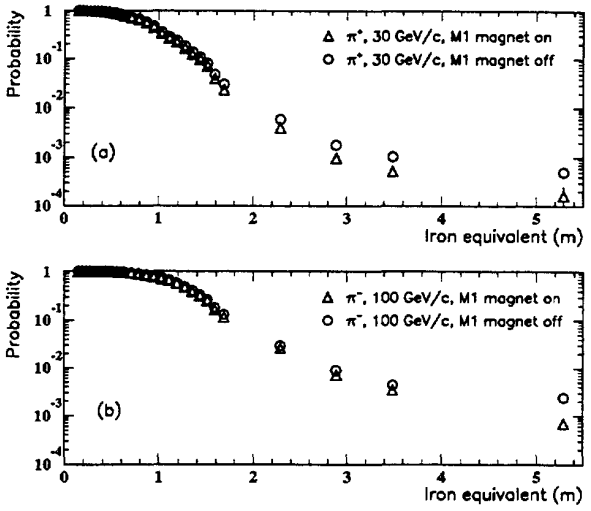

Figure 4: Punchthrough probability as a function of meters of equivalent iron for a) 30 GeV/c π^+ with M1 at full field (3 Tesla) and M1 off and b) 100 GeV/c π^- with M1 at full field and M1 off.

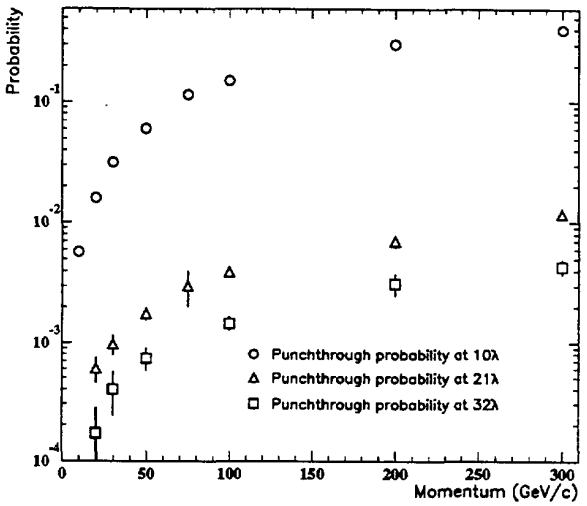

Figure 5: The punchthrough probability at Station 1 (10λ), Station 2 (21λ) and Station 3 (32λ) as a function of the initial pion momentum.

3.2 Punchthrough momentum study

The aim of this analysis is to give a momentum and angular spectrum of punchthrough particles at the depth of 10λ, which can be compared with simulation results for the LHC detectors.

The absorber magnet (M2) of the RD5 setup is used as a muon spectrometer. The muon momentum can be measured with the three large area muon stations that are placed in front of, within and behind the magnet. Each station measures a track in space with a spatial resolution of 1 mm and an angular resolution of 1 mrad. The corresponding momentum resolutions ($\Delta p/p$) are: -8.5 %, $+10$ % for 30 GeV/c and -18 %, $+27$ % for 100 GeV/c.

To be able to fit the momentum, the particle has to give a track in two consecutive muon stations. The minimum penetration depth required is therefore 20 hadronic interaction lengths λ. The momentum is fitted using the GEANE package. The fit results are given for a reference plane at 10λ.

The beam used at RD5 contains a significant amount of muons, mostly from pions that decay before reaching our experimental setup. To reduce this background we cut on the *activity* variable, which is a measure for the shower size in TRACAL (for details see [3]). We declare an event as "pure muon" if the *activity* is below a given threshold, depending on the beam energy. The fraction of events that are identified as muons are given in Table 1.

For further background reduction we also cut on the track position. If the fitted track does not point back to the end of the calorimeter it is rejected. This removes halo muons and also faulty tracks, where due to ambiguities the wrong combination of track segments in the muon stations was selected. We also cut on the number of incoming tracks, measured by the beam chambers, to reject multi-particle events. However, the largest fraction of events do not match the requirement of having a track reaching the second muon station.

In Figure 6 we give the preliminary result for the punchthrough probability as a function of momentum. Here we do not yet apply any acceptance or efficiency correction. The plots include data from a 30, 50, 100 and 300 GeV/c π^- beam. Only data with 10 λ trigger are shown. The data with min. bias trigger give essentially the same result, but with lower statistics. We will add these two data sets in the ongoing analysis.

To normalize the 10 λ trigger we used the measured total punchthrough probability for 10 λ, as described in the previous section. The hole at 0 GeV/c shows the momentum acceptance of our detector, which is about 3 GeV/c.

In Fig. 7 we present the angular distribution of the punchthrough particles. The plots show the slope of the tracks ($\tan\varphi$) in the bending plane behind the TRACAL. The data shown were taken with M1 off, thus the distribution centers at zero.

beam momentum GeV/c	muon contamination		selected events	
	min. bias	10 λ	min. bias	10 λ
-30	3.4 %	49.9 %	0.05 %	0.62 %
-50	1.7 %	22.0 %	0.08 %	1.02 %
-100	1.6 %	9.4 %	0.18 %	1.12 %
-300	2.5 %	5.5 %	0.58 %	1.22 %
+30	1.3 %	35.3 %	0.05 %	0.89 %
+100	2.5 %	11.8 %	0.19 %	0.97 %
+300	9.2 %	19.6 %	0.52 %	0.99 %

Table 1: Muon contamination of data for π^- and π^+ beam and fraction of selected events having a track reaching 20 λ.

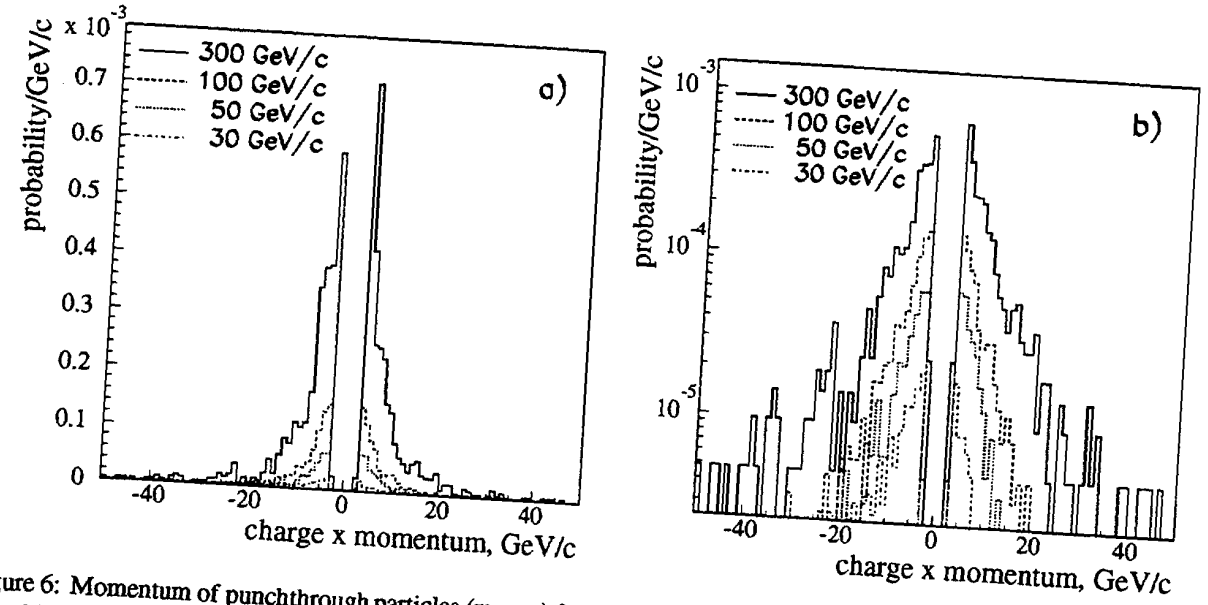

Figure 6: Momentum of punchthrough particles (muons) for different pion beam energies at a depth of 10 λ. With linear a) and logarithmic scale b) (preliminary).

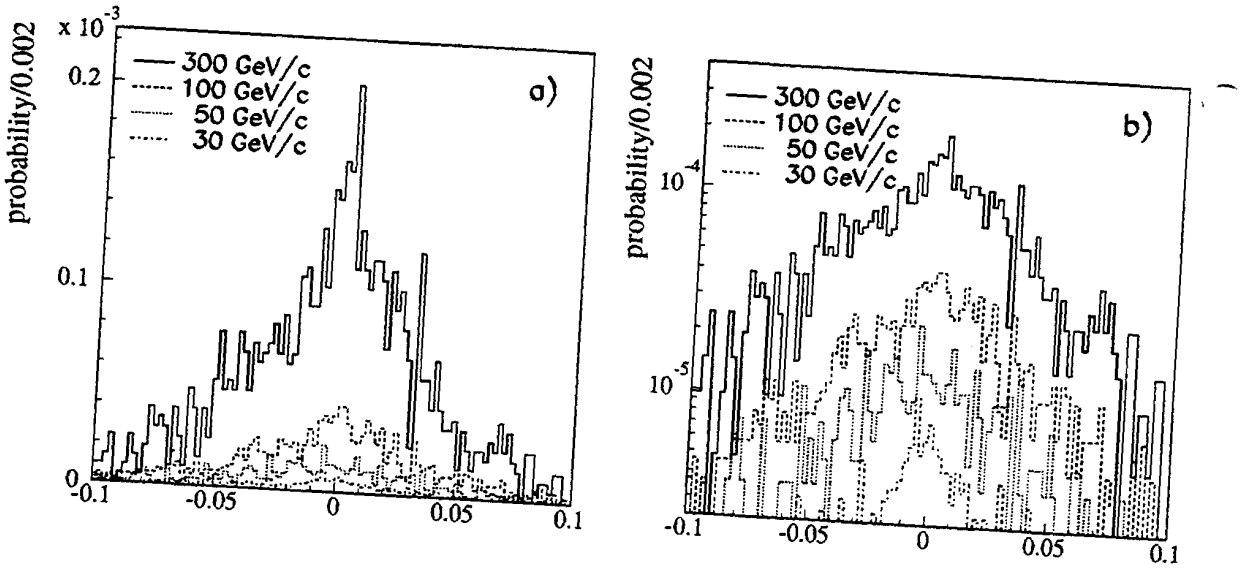

Figure 7: Slope of tracks ($\tan\varphi$) with respect to the beam in the bending plane at 10 λ, with linear a) and logarithmic scale b) (preliminary).

3.3 Punchthrough simulation for RD5 setup

Since results from simulations must necessarily be heavily relied upon in the design of muon detectors for hadron colliders, it is important to validate these simulations by comparing their predictions with real data. RD5 provides unique opportunities for this purpose. Simulation of the experiment has been done for the 1991 geometry, including the TRACAL, RPCs, muon drift chambers, M2 toroidal magnet with field, and M1 magnet geometry (but so far without field in M1). The 3.15 version of GEANT was used for the simulation [12]. Negative pions of 30, 50, 100, and 300 GeV/c momenta were simulated using both the GHEISHA and FLUKA packages for hadronic interactions (Table 2 gives the number of triggers for each). The energy cutoffs used were 1 MeV for all types of particles in the absorbers, and 10 keV for electrons and γ's in the sensitive parts of the detectors. The lower cutoffs in the sensitive detectors allowed neutral particles to interact and produce low-energy electrons which could then be counted as hits. Hits were registered by any charged particle with energy greater than 10 keV. Processes that were part of the simulation were pair production, bremsstrahlung, delta-ray production, photonuclear fission, photo-electric effect, Compton scattering, Rayleigh scattering, and muon-nuclear interactions. The analysis of the simulated data was done in three different ways which all gave good agreement (consult reference [13] for further information about these and other details of the simulation). The results shown here are from the method which digitized all charged particles and wrote a raw data file which was subsequently analyzed by the same analysis program as was used for the real data.

Momentum	Hadronic Package	Triggers
30 GeV/c	GHEISHA	8050
50 GeV/c	GHEISHA	6850
100 GeV/c	GHEISHA	6275
300 GeV/c	GHEISHA	3010
30 GeV/c	FLUKA	11250
50 GeV/c	FLUKA	7415
100 GeV/c	FLUKA	6600
300 GeV/c	FLUKA	1440

Table 2: Number of simulated π^- triggers.

Figure 8 shows the total punchthrough probability versus depth for real data and GEANT 3.15 simulation, using GHEISHA for hadronic interactions. Figure 9 shows real data and simulation results using FLUKA for hadronic interactions. Both simulations underestimate the amount of punchthrough compared to the real data, although the agreement in case of FLUKA is significantly better than with GHEISHA. Figure 10 is an enlargement of the 50 GeV/c real data and both types of simulation for depths below 10λ. The dotted line shows that lowering the CUTHAD, CUTNEU, and CUTGAM cutoffs for hadrons, neutrons and γ's from 1 MeV to 10 keV in the absorbers did not significantly improve the agreement of the GHEISHA results with the real data. An analysis of the simulated particle identities in one of the detectors, at 1.19 m of iron was done for a sample of data. The most distinctive difference between the profiles for FLUKA and GHEISHA was that 50% of the FLUKA punchthrough events contained protons compared to 32% for GHEISHA, and over half the excess punchthrough events given by FLUKA were from showers containing only protons [13]. A more detailed study of this difference is underway, it should be stressed, however, that the accuracy already achieved is adequate to make predictions for LHC.

3.4 Study of muon induced secondaries

High energy muons (of the order of 10^2 GeV) traversing matter produce a significant amount of electromagnetic secondaries by knocking-on electrons, bremsstrahlung and direct production of e^+e^- pairs. This radiation of secondaries near the muon track may jeopardize the precision of the muon track measurement. It is therefore important to study the production of electromagnetic secondaries by muons and its impact on muon detection. Muon induced secondaries were studied at RD5 with different geometries (various distances from the absorber) and with different detector types (SiBT, HSC, DTBX, WLDC).

3.4.1 Identification of muon induced electromagnetic particles in TRACAL

Influence of the muon induced secondaries on the performance of the HSC was studied with single-layer HSCs in TRACAL. In HSC the coordinate perpendicular to the wire is determined by the distribution of charge induced on the strips. A selection of strips carrying the largest charge (Q_{middle}) was made after calibration of the raw ADC data. The charges carried by both its neighbours were defined as Q_{left} and Q_{right}. A threshold was applied to the sum of the three signals.

The observed distribution of the ratio Q_{right}/Q_{middle} versus Q_{left}/Q_{middle} (for a single layer) is plotted in Figure 11. This distribution is expected to be lying within the range – which is obtained from simulation – indicated by the solid lines in Figure 11. The entries above the curve are indicative of a charge distribution wider than that expected for a single muon track. We attribute these entries to the superimposed charge distributions of a muon and one or more electrons

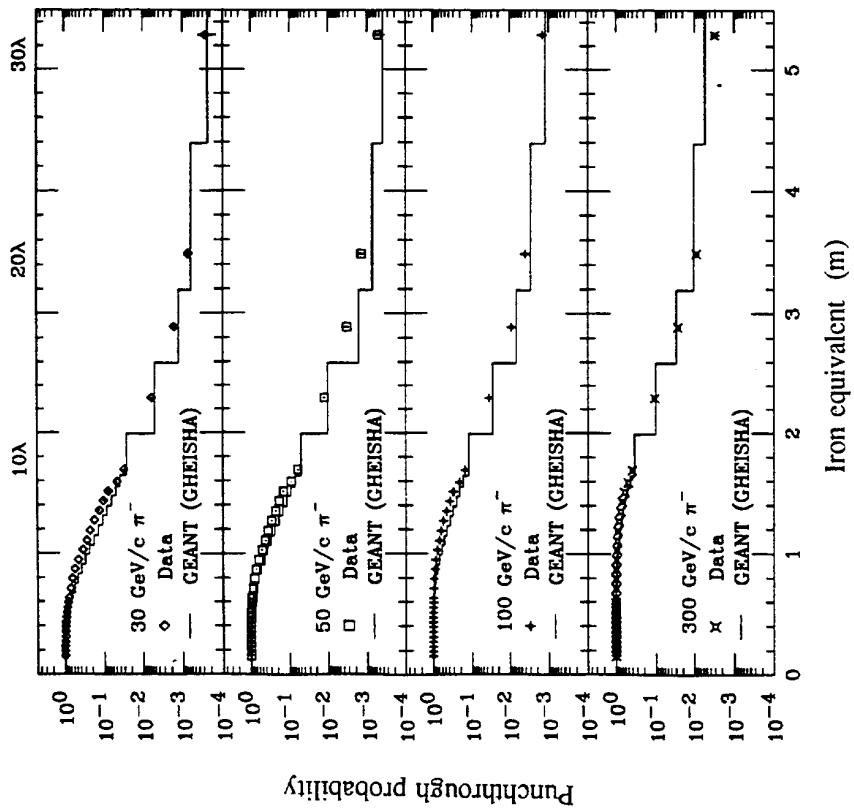

Figure 8: Total punchthrough probability for 30, 50, 100, and 300 GeV/c π^-'s, showing real data and simulation with GHEISHA.

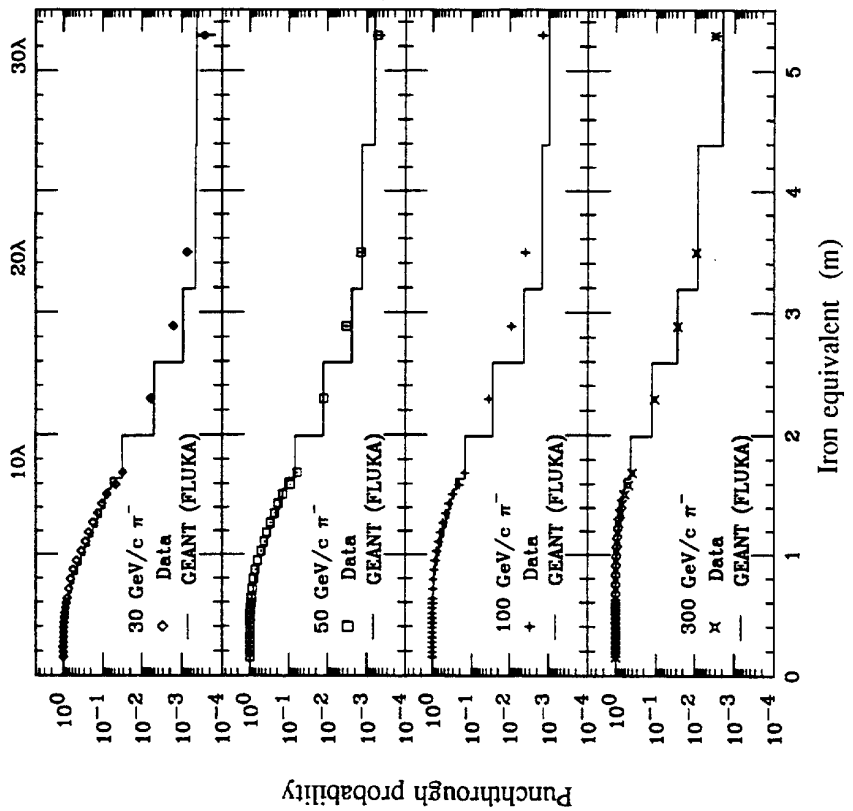

Figure 9: Total punchthrough probability for 30, 50, 100, and 300 GeV/c π^-'s, showing real data and simulation with FLUKA.

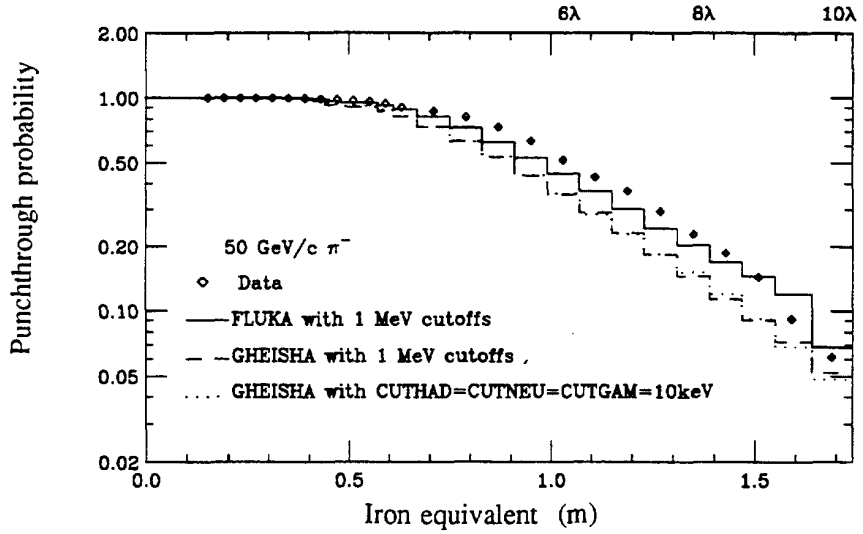

Figure 10: Comparison of 50 GeV/c real data and simulation with FLUKA and GHEISHA with 1 MeV cutoffs, and GHEISHA 50 GeV/c simulation with CUTHAD=CUTNEU=CUTGAM=10 keV.

created in the absorber by the primary muon. The probability for measuring an incident muon accompanied with one or more electrons is in the order of 15 % for 20 GeV/c incident muons and is increasing up to 25 % for 300 GeV/c muon momentum. These percentages are obtained from the number of entries above the expected range, normalized by the total number of entries in this Q_{right}/Q_{middle} versus Q_{left}/Q_{middle} plot.

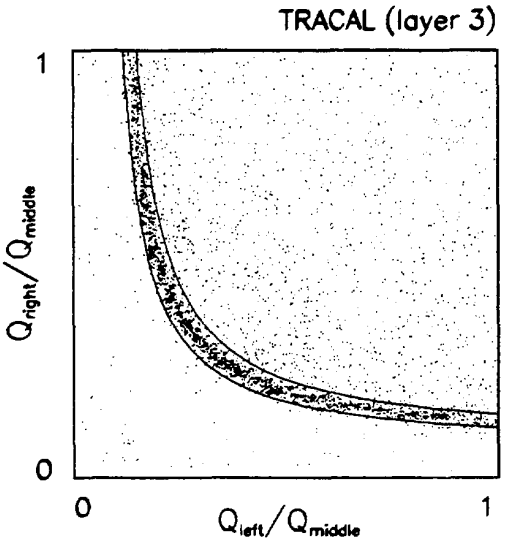

Figure 11: The ratio Q_{right}/Q_{middle} plotted against Q_{left}/Q_{middle} for a single-layer HSC. The entries above the expected range (solid lines) are clearly visible.

Confusing multi-track measurements can be recognised and a cut can be performed to remove events with too broad charge distributions. Therefore, the strip information is a powerful tool for muon track reconstruction. The height of the charge signals is usually large for contaminated events, and the position of the centre-of-gravity of the charge distribution is off the incident track.

More detailed analysis related to electromagnetic showers is still in progress. The topics under investigation invoke the influence of the following parameters to electromagnetic shower production and observation in TRACAL:

- different types of absorber material, i.e. different interaction lengths,
- different distances between absorber and a single-layer HSC,
- several magnetic field strengths.

3.4.2 Detection of muon induced secondaries with DTBX using the mean-timer method

The production of soft δ-rays and el.-mag. showers can be measured using arrays of staggered drift tubes. Let us consider a three layer array of drift tubes and assume a linear space-time relationship, accurate wire positioning and accurate layers staggering. The drift times in consecutive cells originate from a particle crossing at normal incidence, as in Figure 12a,

and satisfy the relation $t_M = t_A + t_B$ and $t_M = t_B + t_C$ where t_M is the maximum possible drift time. If the track is inclined the relations are $t_M = t_D + t_E - \Delta t(\theta)$ and $t_M = t_E + t_F + \Delta t(\theta)$ as can be argued for Figure 12b. So using three layers, to correct from systematic errors coming from muon inclination, the sum $t_M = (t_D + 2t_E + t_F)/2$ is a constant.

This kind of technique was used in RD5, in the DTBX prototype [5] (see also Sec. 5.6) exposed to muon beams of 100, 200, 300 GeV/c momentum. The distribution of t_M for a typical triplet of tubes at normal beam incidence is shown in Figure 14 where the time origin is set to zero. We can see that, apart from the expected peak due to ideal muons, there is a long tail towards negative values. This tail may have several causes: noise, electric field shaping, cross-talk, double beam tracks, and muon induced secondaries. Noise and cross-talk were found to be negligible, while cell uniformity was checked with a fine scanning through it.

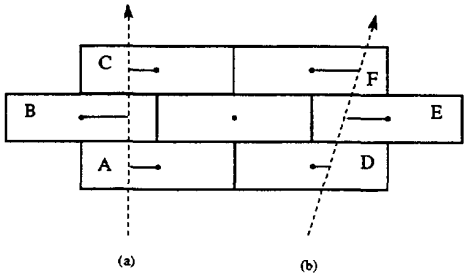

Figure 12: Principle of mean-timer operation

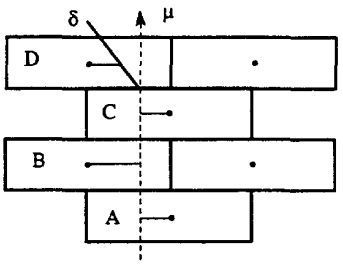

Figure 13: δ-ray seen by mean-timer system

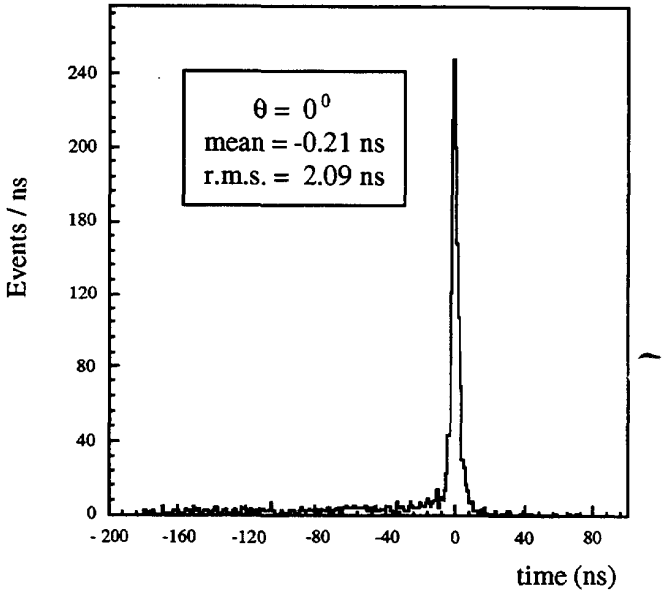

Figure 14: Time resolution of DTBX with mean-timer method at 300 GeV/c μ^- beam.

It has been found that the affected events can be divided into two classes: single hits coming too early to be caused by the primary muon and events with hits in more then one cell per layer. We interprete the first class as soft δ-rays and the second one as electromagnetic showers. The shower interpretation is supported by the fact that a few subsequent layers were hit.

In the analysis we first selected events with showers. Identification of δ-rays is done in the remaining sample. Let us extend our considerations to a four layer system (Figure 13). If we consider $t_{M1} = (t_A + 2t_B + t_C)/4$ and $t_{M2} = (t_B + 2t_C + t_D)/4$ we see that there is a correlation between this two quantities depending on where a δ-ray is produced. In fact a δ-ray produced in plane A or D will affect only t_{M1} or t_{M2}, while a δ-ray produced in plane B or C will affect both of them. This is clear in Figure 15 where t_{M1} is plotted against t_{M2}. The data points are distributed along four equally spaced lines showing that most of the δ-rays produced are contained in a single cell: in fact the previous argument does not hold in presence of δ-rays crossing more than one cell. The very good time resolution allows identification if $t_M \geq 4\sigma = 15$ ns (equivalent to $\sim 800\mu$m two track separation) off the peak centre. The data for showers and single δ-ray production are summarized in Table 3. Only a small fraction ($\sim$20 %) of δ-ray events was also seen in more than one layer. The δ-ray production is constant in the investigated muon momentum range, while the shower probability is slowly rising with energy. Corrections for detection efficiency and double beam tracks ($\sim$2%) in coincidence in the same event, identified as parallel tracks, were applied to get the right estimation of the fraction of processes.

p (GeV)	δ-rays per cell	el.-mag. showers
100	5.7 ± 0.2 %	3.9 ± 0.3 %
200	5.5 ± 0.2 %	5.5 ± 0.4 %
300	5.9 ± 0.2 %	6.4 ± 0.3 %

Table 3: Fraction of δ-rays and el.-mag. showers. The fraction of δ-rays is computed per cell of 2 cm drift space and at $d > 800\mu$m distance from the muon position in the drift direction.

The fact that the identification of the δ-ray is obtained from the time information allows to compute the distance of the produced electron from the incoming muon along the shortest drift path to the anode wire. The distribution of this distance is shown in Figure 16.

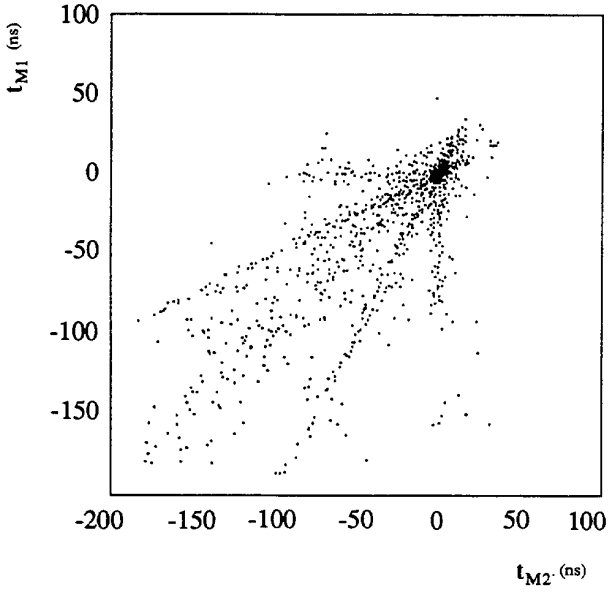

Figure 15: Correlations of two mean-timers in presence of δ-rays

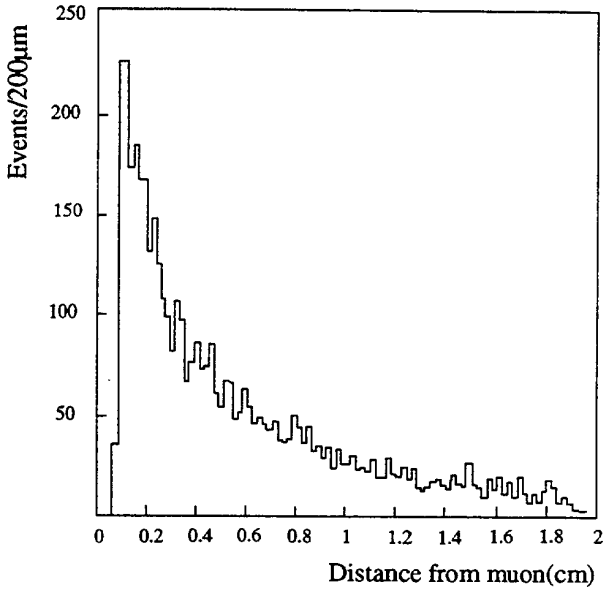

Figure 16: δ-ray distance from the primary muon

3.4.3 Electromagnetic showers in WLDC

The electromagnetic shower studies in the WLDC are done in two parts. The first part deals with the recognition of contaminated tracks. The next step is to determine whether the reconstructed track matches to the real muon track through the chamber.

The presence of e.m. secondaries in the WLDC is recognized after the track reconstruction by observing the 'signed residua', i.e. the distance between hit and reconstructed track. The residua are given a negative sign if the hit is nearer to the anode than the reconstructed track. The distribution of the signed residua shows an asymmetric tail (Fig. 17). The signed residua from the full simulation show the same tail as those from the data (Fig. 18). If no secondaries are produced, the distribution is not asymmetric, as also shown in Fig. 18. Hence the hits in the tail are caused by δ-electrons and other secondaries. Due to the pulse length in the WLDC, a hit from a δ-electron passing the chamber nearer to the anode than the muon masks the muon hit. The fraction of hits with a residuum larger than 600 μm is $\sim$ 9% (taken from Fig. 17, no cuts needed). The fraction of tracks with hits in the asymmetric tail is given in Table 4. The first column shows that about 71 % of such 8-point tracks are undisturbed. About 19% of the tracks are impaired by one or two δ-electron hits and the rest by more than 2 hits.

energy of muon		number of hits outside 3 σ			
		0	1	2	more than 2
10 GeV	data	72.6	9.6	9.1	8.7
	simulation	75.0	11.4	7.0	6.6
50 GeV	data	67.8	11.2	10.9	10.1
	simulation	72.0	12.5	7.8	7.7
100 GeV	data	71.0	10.5	8.3	10.2
	simulation	72.4	11.2	7.5	8.9
200 GeV	data	67.6	11.8	8.6	12.0
	simulation	71.1	10.3	8.1	10.5

Table 4: Fraction (%) of 8-hit tracks with n residua larger than 3 σ of the single hit resolution for WLDC data and simulation.

The second part of the studies requires an external definition of the muon track to compare it to the reconstructed track in the WLDC. Here the information from the first muon station is used. A muon track from the first muon station is required to have a χ^2/dof better than 3, to be triggered by the 2 $\times$ 2 cm^2 trigger counter and to be located within 2 cm from the beam axis at the first muon station. Such tracks are taken as reference for comparison with the track reconstructed in the WLDC. A WLDC track deviating more than 4σ from this external muon track in angle or position is called 'non-matching'. To test this, a variable $R = \sqrt{(\frac{\Delta x}{4\sigma_x})^2 + (\frac{\Delta\theta}{4\sigma_\theta})^2}$ is defined. A value of $R < 1$ is required for 'good matching'. Table 5 gives the fraction of non-matching tracks for different data samples. The number of non-matching tracks is correlated to the number of bad hits. This demonstrates, that large residua in the (local) track reconstruction indicate well the matching quality. The idea to reject a hit with a residuum worse than 3 σ of the single hit resolution and

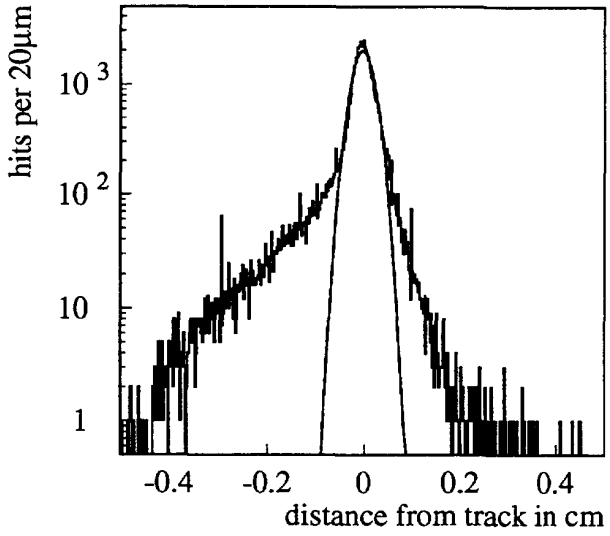

Figure 17: WLDC Data (200 GeV muons): Signed residua of a reconstructed muon track, with logarithmic scale to show the asymmetry. The anode is on the left side. A fitted gaussian is also shown.

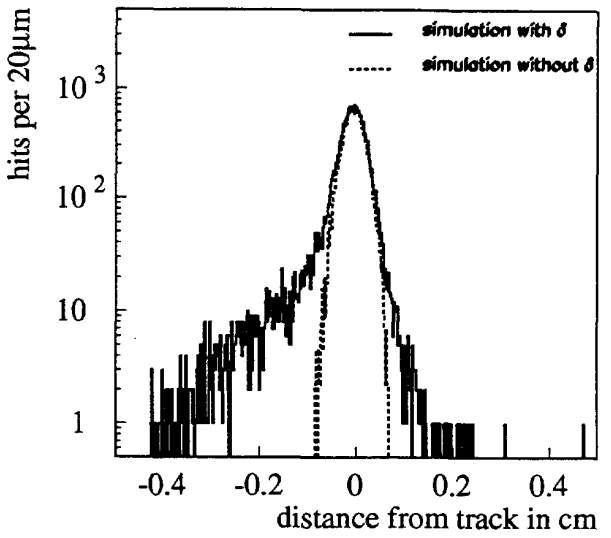

Figure 18: WLDC Simulation (200 GeV muons): Signed residua of reconstructed tracks, with logarithmic scale to show the asymmetry. The solid line is the simulation including δ-electrons, the dotted line is the simulation without generation of secondaries.

energy of muons	quality of reconstructed track			
	all residua $< 3\sigma$	one residuum $\geq 3\sigma$	two residua $\geq 3\sigma$	more than two residua $\geq 3\sigma$
10 GeV	0.7±0.4	11.7±3.9	13.2±5.0	28.3±7.8
30 GeV	0.4±0.2	2.5±1.3	13.1±3.2	51.3±6.6
50 GeV	0.6±0.2	2.9±1.3	15.4±3.6	41.0±5.9
100 GeV	0.5±0.3	3.8±2.2	14.8±4.9	47.6±8.7
200 GeV	0.5±0.2	1.2±0.6	15.3±2.4	49.6±4.4

Table 5: Fraction (%) of tracks in WLDC not matching the external muon track. The matching criterion is $R < 1$. Good tracks (all residua $< 3\sigma$) do always match the external measurement.

to reconstruct the track again may help to recover some of the mismatching tracks.

3.4.4 Study of electromagnetic showers with silicon detector

A dedicated study of electromagnetic showers generated by high energy muons passing through dense materials has been performed in 1992 and 1993 using the SiBT placed behind an absorber. The main goal of this study was to check the predictions of the GEANT simulation program. The very good spatial and two track resolution of the silicon microstrips detectors enabled us to distinguish the electron hits from those of muons down to a distance of 100 μm. During these experiments the 40 cm thick iron mirror was used as absorber. For that purpose it was moved into the beam. When data without absorber were taken for comparison, the irron mirror was put back into its original position so that the beam could pass through the hole in the centre of the mirror.

Data were taken with μ^- beams of 50, 100, 200 and 300 GeV/c momenta, both with and without the iron absorber in front of the silicon telescope. To measure the fraction of muon tracks which are accompanied by electromagnetic showers we have to distinguish the secondaries coming from the iron absorber from those generated in silicon planes. Data taken without absorber have been used for this purpose. The contribution of the noise of the detectors has been estimated using pedestal runs. This type of noise could be reduced well below that coming from muon interactions in silicon by a cut on the cluster size and on the signal over noise ratio (S/N) of each cluster. This cut does not reduce the efficiency for genuine muon hits.

The measured data have been compared with the results of a simulation program based on GEANT 3.15. In the Monte Carlo the electrons and photons generated by the μ passage through dense materials are tracked until their kinetic energy falls below 100 keV. The Monte Carlo program includes also a detailed simulation of the detector response. The simulated events are then reconstructed and analyzed with the same analysis chain as used for real data.

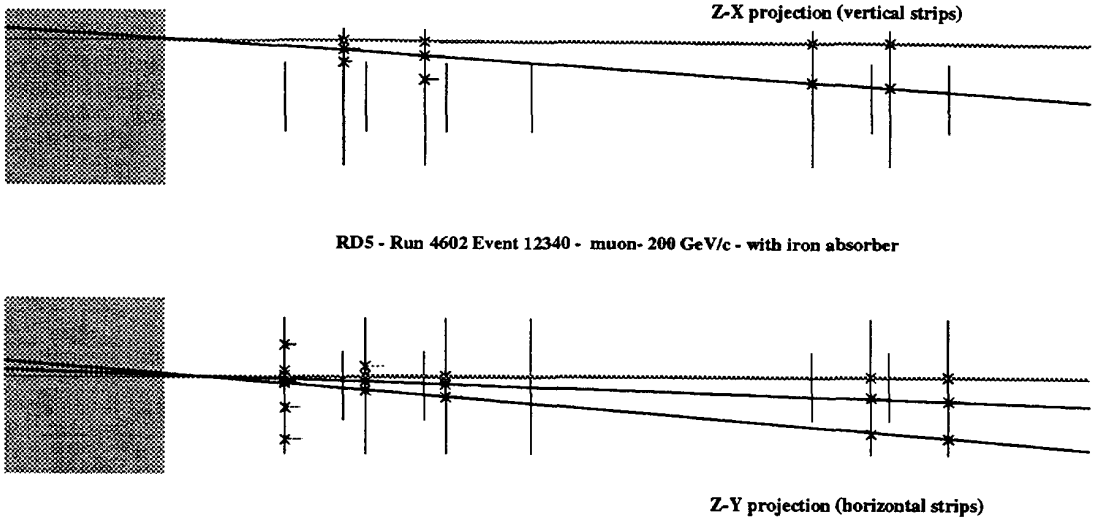

Figure 19: Display of one event in which a 200 GeV/c muon (dotted track) has generated two δ rays of which one is reconstructed in both projections.

In the analysis the two different projections of the SiBT are treated separately. Due to the different geometrical acceptance of the two projections and the absence of stereo layers, no attempt has been made to reconstruct the tracks in space. Nevertheless, events in which a second track accompanies the muon track can be easily identified, as shown in fig. 19.

The first step of the analysis is to require the presence of a muon track reconstructed in the SiBT and confirmed in the subsequent detectors. If more than one track is reconstructed in the silicon telescope the one with the smallest difference from the average beam direction is taken. In each plane with a hit linked to the muon track we look for additional hits that satisfy the cuts on the cluster size and on the S/N ratio, and measure the distance of the center of the cluster from the extrapolated muon track. At the same time we count the number of events which have additional hits on the silicon planes and measure their multiplicity. In Fig. 20 we show, both for the data and the simulation, the fraction of events which have at least one additional hit in a plane at a distance between 100 μm and 2.5 cm (the lower limit being given by the two track resolution and the upper one by the detector acceptance) as a function of the distance of the silicon plane from the iron absorber and for different beam energies. These distributions are obtained subtracting the contribution of secondaries generated in silicon planes. The distributions show that the fraction of events with additional hits in the detectors increases with energy, as expected from the behaviour of the muon energy loss. The decrease of the fraction of events with additional hits when moving away from the iron absorber is due both to the geometrical acceptance and to the absorption of electrons and photons in the 500 μm thick silicon planes and is well reproduced by the simulation.

In Fig. 21 we show the distribution of the distance of additional hits from the μ track, comparing again the data and the simulation, after the subtraction of data taken without absorber. Also shown is the distribution of the number of additional hits in a silicon plane due to the electromagnetic interactions of the μ in the iron absorber.

The GEANT Monte Carlo prediction agrees quite well with the data at different energies and at various distances from the iron absorber. Also, the distribution of the background hits around the muon track is well reproduced. We are thus convinced that the GEANT simulation of the environment of a muon momentum measurement chamber can be used with some confidence.

3.4.5 Conclusions

The results presented above demonstrate that the presence of secondaries can be clearly recognized by the detectors.

However comparing the exact numbers one has to keep in mind that a classification of the observed phenomena (e.g. soft δ-rays and el.-mag. showers) is somewhat arbitrary. Production of the secondaries vary significantly with the geometry of the detector and results of measurements depend strongly on the exact definition of quantities in question. Therefore muon chambers have to be tested in the configuration as close as possible to the final detector. The RD5 setup provides such a possibility and we are going to continue the study next year with new prototypes.

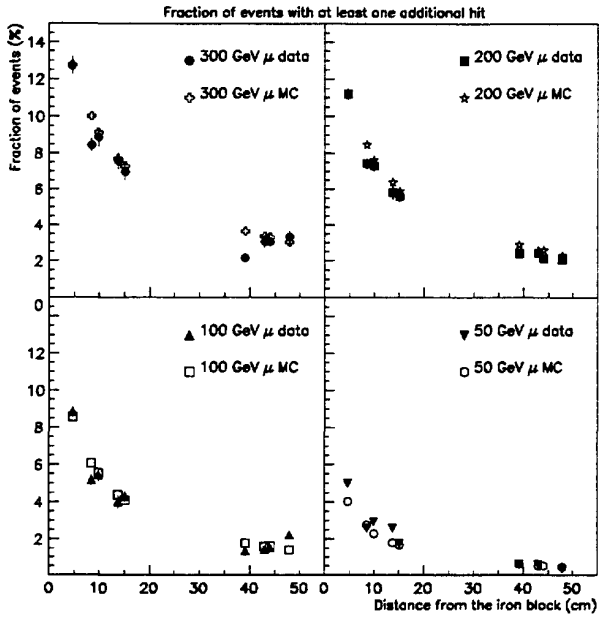

Figure 20: Fraction of events with additional hits in the silicon planes versus the distance of the plane from the iron absorber for different beam energies.

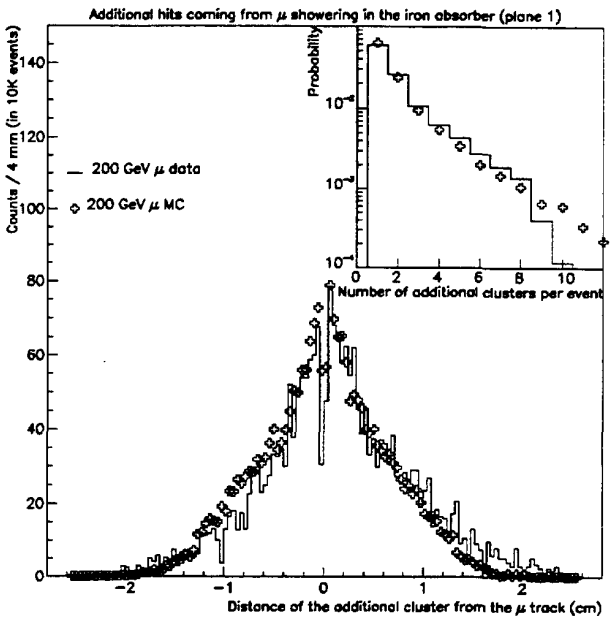

Figure 21: Distribution of the distance of additional hits due to showering from the μ track. In the small frame we show the probability distribution of the number of additional hits.

4 Muon Trigger Study

A fast and efficient muon trigger system is a crucial part of any LHC experiment. The RD5 setup provides a facility to test trigger devices in the environment close to that at LHC. In the period of 1992-93 three different trigger processors have been tested.

4.1 Pattern Comparator Trigger (PACT)

The Pattern Comparator Trigger is a device being developed for the first level muon trigger of the CMS detector [15]. The first PACT processor prototype has been tested in a laboratory and then in the RD5 experiment during the August/September '93 run. The aim of the test was to check the feasibility of the design and its ability to run with high speed. Three programmable ALTERA 7128 chips were used in the processor housed in a VME module.

The processor uses information from the RPCs, which are part of the RD5 setup. The chambers are placed in the field of the RD5 absorber magnet M2 which simulates the magnetic field in the return yoke of CMS. Four chambers with horizontal strips were selected and their digital outputs were fed into the processor. The trigger decision is based on patterns of hits which were chosen using data from previous RD5 runs. Seven groups of patterns were defined corresponding to momentum thresholds of 10, 20, 30, 50, 75, 100 GeV and infinity (straight tracks). The processor responds with the pattern group number or with zero if no match is found in an event. In case where several matching patterns are found in the event (due to a large cluster size in some of the chambers) the group number corresponding to the maximum momentum is selected.

The data are processed continuously with the speed of an external clock. The processor reads data from the RPCs and processes them during 4 clock ticks. When the RD5 triggering signal arrives the data are read by the Data Acquisition computers. The clock period of 60 ns has been used in this test but the module was earlier tested in a laboratory with a 25 ns clock i.e. with the speed required by the LHC. In both cases we experienced no losses due to timing.

The PACT processor was tested in the beam at four energies: 20, 30, 50 and 100 GeV. In the offline analysis it was checked that the response is in agreement with what we expect it to be from the direct readout of the RPC strips. This agreement is obtained in 100% of the events.

The trigger efficiency as a function of the beam energy was measured for different thresholds. The steepness of the obtained curves is not yet satisfactory. We attribute this fact to the geometrical configuration, segmentation and the cluster size of the used RPCs that were not yet optimized for this study. The tests will be continued next year with an improved setup. The current version of the PACT processor requires signals from all four chambers to give an answer. In order to be able to deal with detector inefficiencies we plan to include patterns corresponding to cases, when one of the chambers is missing.

4.2 Coincidence Matrix Trigger Processor

A prototype of a first level muon trigger that exploits the information of two RPC planes has been built in Rome [18] and tested during the September 1993 run period. The guidelines for the design are:

- time tagging with 6.25 ns resolution, i.e. 1/4 of the LHC bunch crossing period;
- multi-threshold capability;
- fixed response time of less than 200 ns.

The processor consists of a 32×32 coincidence matrix, a counter, a cluster encoder and a memory. The matrix is made of an array of four GaAs cross-point switches that map the first plane onto the second plane. With such an arrangement, up to thirty two 4-strip wide, or four 32-strip wide roads can be implemented simultaneously. Whenever a pattern is accepted by the coincidence matrix, i.e. the lowest momentum threshold is passed, a trigger signal is sent to the counter and the two hit patterns that satisfy the coincidence are latched into two 32-bit registers. The counter tags the time reponse of the coincidence matrix relative to the experiment trigger. The processor is designed to operate with a 160 MHz clock synchronized with the bunch crossing frequency, but in RD5 a 133 MHz clock was used. The cluster encoder receives the content of the two registers, computes the center of the clusters and compares the two coordinates with different momentum thresholds in a look-up table. The time tag, the coordinate and the momentum information is loaded into a memory. The link of the processor to the data acquisition system is done by a control unit via optical link.

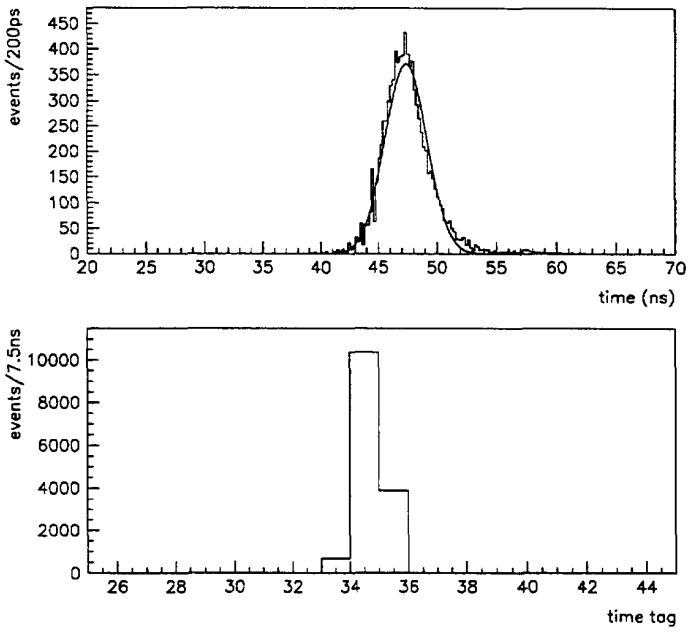

Figure 22: Time distribution of the trigger signal (a) and of the time tag (in ns) encoded by the processor (b).

The input to the processor was provided by the last two RPC planes in Station 3: Y11 and Y12. This configuration gives little sensitivity in momentum, but was chosen for easiness of access to the detectors and to exploit the good performance of double-gap RPC. The Fast-OR signals of the two RPC, the signal from the trigger processor and of the time defining scintillator of the RD5 trigger were recorded on TDC when the processor was operational. Data were taken with 20, 30, 50 and 100 GeV/c momentum muons. Fig. 22 shows the time distribution of the trigger signal and of the time tag encoded by the processor. The time resolution of $\approx$ 2 ns shows that the time response of the RPC is fully preserved by the processor and no additional jitter is introduced: 99.4% of the triggers are tagged in a time interval of three bins corresponding to 22.5 ns. The processing time is 110 ns, mainly due to the cluster and momentum encoding. The cross-point switch matrix has a signal propagation time of $\approx$ 2 ns. Fig. 23a shows the distribution of the difference of the coordinates, $\Delta y = y_{12} - y_{11}$, for muon momenta of 30 and 100 GeV/c. As said before, the chosen configuration has poor sensitivity: if we add the information of one RPC plane in Station 1 and compute the difference $\Delta y' = y_1 - (y_{11} + y_{12})/2$, then we exploit the bending power of the toroid and gain in sensitivity as shown in Fig. 23b.

4.3 Resistor Matrix Trigger

The Weighting Resistor Matrix (WRM) is a conceptually very simple trigger processor based on a resistor network. It is capable to recognize an experimental pattern on the basis of a non integer weight that measures the "difference" between an experimental pattern from a set of ideal patterns defined in the processor [19]. In the test described below a WRM prototype connected to five RPC chambers was used to simulate a stand-alone muon trigger for an LHC experiment. The purpose of the test was to measure the muon trigger efficiency of the processor and its rejection power for hadronic

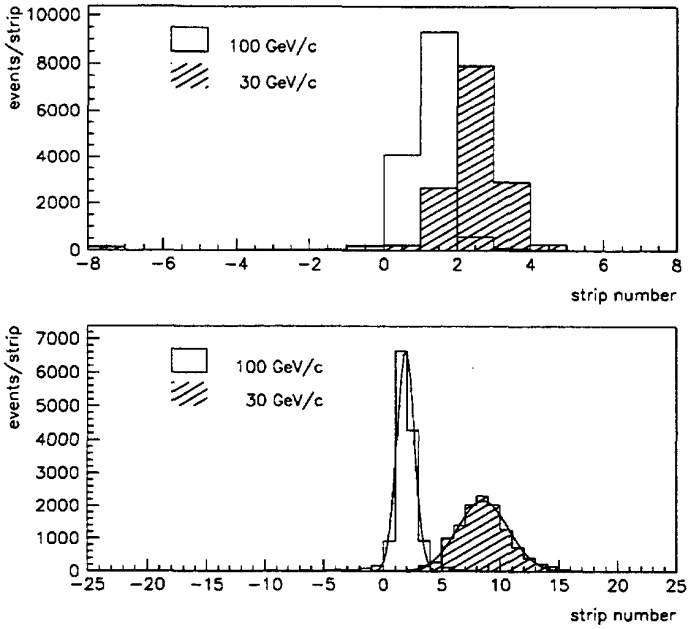

Figure 23: Momentum encoded by the processor using only the two RPC planes in Station 3 (a) and using also one RPC plane in Station 1 (b).

showers. The RPC chambers connected to the processor were reading the z-coordinate which is not affected by the magnetic field. Therefore the typical muon pattern was that of a straight track which had to be discriminated against the more complicated pattern of a hadronic shower. A WRM trigger processor could also be designed for the case of muon trajectories bent by the magnetic field.

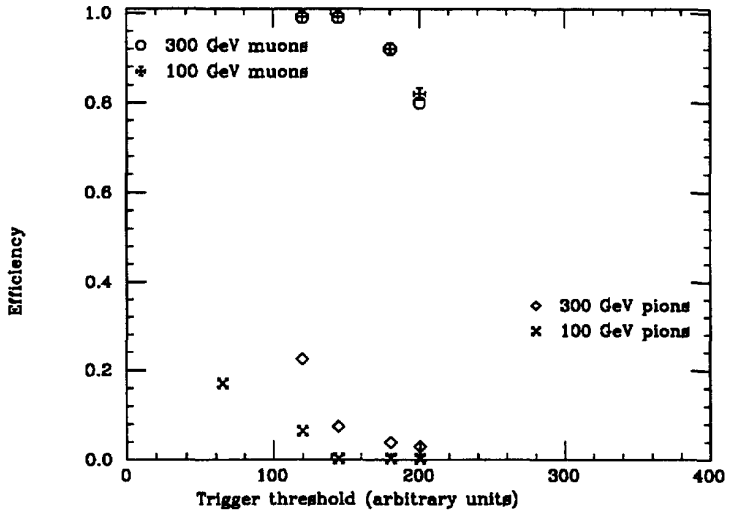

Figure 24: The muon recognition efficiency and the probability of a pion to be accepted as a muon

During the tests signals of 32 central strips of the RPCs Z1, Z2, Z5, Z6, and Z7 were sent into a 32×10 WRM conceived to recognize the pattern of a straight trajectory characterized by 7 different slopes with respect to the beam line. For a given experimental pattern the output of the trigger circuit is a voltage level proportional to the weight of each of the 7 muon patterns. The signal is then digitized in the data acquisition system. The event is accepted as a muon if the maximum weight exceeds a certain threshold. The muon recognition efficiency and the probability of a pion to be accepted as a muon are shown in Figure 24 versus the weight threshold.

5 Chamber Tests

Four weeks of RD5 beam time were devoted to chamber tests and a large amount of tests were done parasitically during RD5 physics runs.

Chambers tested in RD5 might be devided into two groups: fast chambers for triggering, like RPC, PPC, FireFly, and precise chambers for tracking like Silicon Strip Detector, WLDC, DTBX, CSC, HSC. However, from the point of view of tests, most of the questions to be studied are common for both groups e.g. efficiency, space and time resolution, response uniformity, and noise for various gas mixtures, high voltage values, incident particle fluxes etc. In this section we can give only a very brief summary of this part of the RD5 activity. For details we refer to RD5 technical notes and ongoing publications.

5.1 Resistive Plate Chambers

The requirements for detectors to be used in the first level muon trigger in experiments at the LHC are:

- good uniformity of response over large areas;
- full efficiency and good time resolution at particle fluxes up to about 100 Hz/cm^2;
- easiness of segmentation;
- small sensitivity to low energy neutrons and photons;
- low noise rate.

The analysis of the RD5 data has shown that many of the above requirements can be met by RPCs built with plates of phenolic polymer. We present new results on the performance of double-gap RPCs and of RPCs operated at low gain with high quenching gas mixtures. We have also studied the space resolution of RPCs reading the charge induced on the strips and reconstructing the impact point with the center of gravity method.

5.1.1 Double-Gap RPC

A double-gap RPC consists of two separate chambers, built with the same technique described in detail in reference [6], and assembled as shown in Fig. 25. A single read-out plane, segmented in strips 2 m long and with 3.1 cm pitch, is placed between the two chambers to pick-up the signal from both gas volumes. The two chambers are staggered by 5 cm so that the spacers do not overlap. The strips are read out with the same front-end electronics used for single-gap RPC, thus the effective threshold is halved and this reflects in a better performance at large particle fluxes. The new RPCs are built with "low" resistivity [6, 16] bakelite plates: $\rho \approx 4 \cdot 10^{10}\ \Omega\times$cm.

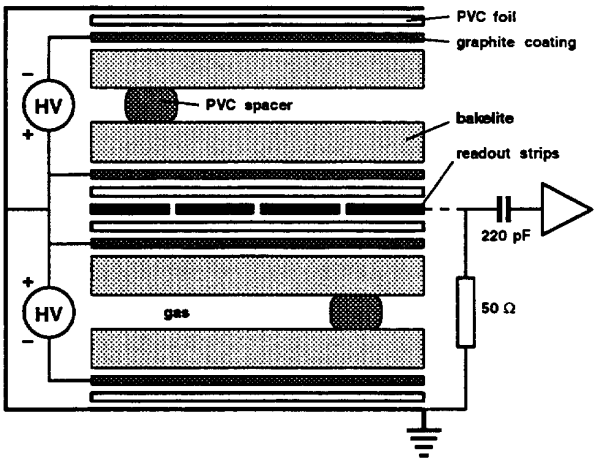

Figure 25: Section of a double-gap RPC.

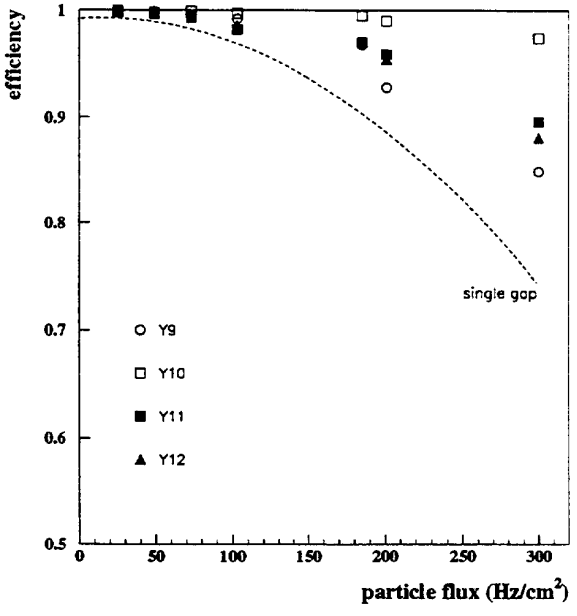

Figure 26: Efficiency as a function of the particle flux of the four double-gap RPC planes (Y9, Y10, Y11, and Y12) compared with the average behaviour of single-gap RPC.

The double-gap RPCs were operated with a gas mixture of 58% argon, 38% butane and 4% freon. The operation voltage, common to the two gaps, was in the range 7.2–7.5 kV: a few hundred volts above the beginning of the efficiency plateau. Measurements of the efficiency and of the time resolution were done with 200 GeV/c muons as a function of the

particle flux. The local flux traversing the RPC was defined by the rate of the trigger scintillators and the beam profile measured with the drift chambers at the positions of the RPC.

At low particle flux, $\approx$ 10 Hz/cm^2, all RPCs reach an efficiency of 99% or higher. Fig. 26 shows the efficiency of the four double-gap RPCs (referred to as Y9, Y10, Y11, and Y12) as a function of the flux, compared with the average behavior of single-gap RPC made of bakelite plates with the same resistivity. We have also studied the behavior of the efficiency as a function of the particle impact point on the detector and we have verified that the reduction in efficiency is localized where the particle flux is larger and that it does not affect the performance of the detector in the adjacent regions.

The time response has been studied by measuring the delay between the signals of the trigger hodoscope and those of the Fast-OR of each plane. We noticed a small systematic difference in the time response of the single strips, but no attempt was made to correct for this effect, neither to correct for the jitter of the trigger signal. On the basis of the four independent measurements, we estimate a r.m.s. contribution of 0.9 ns from the trigger.

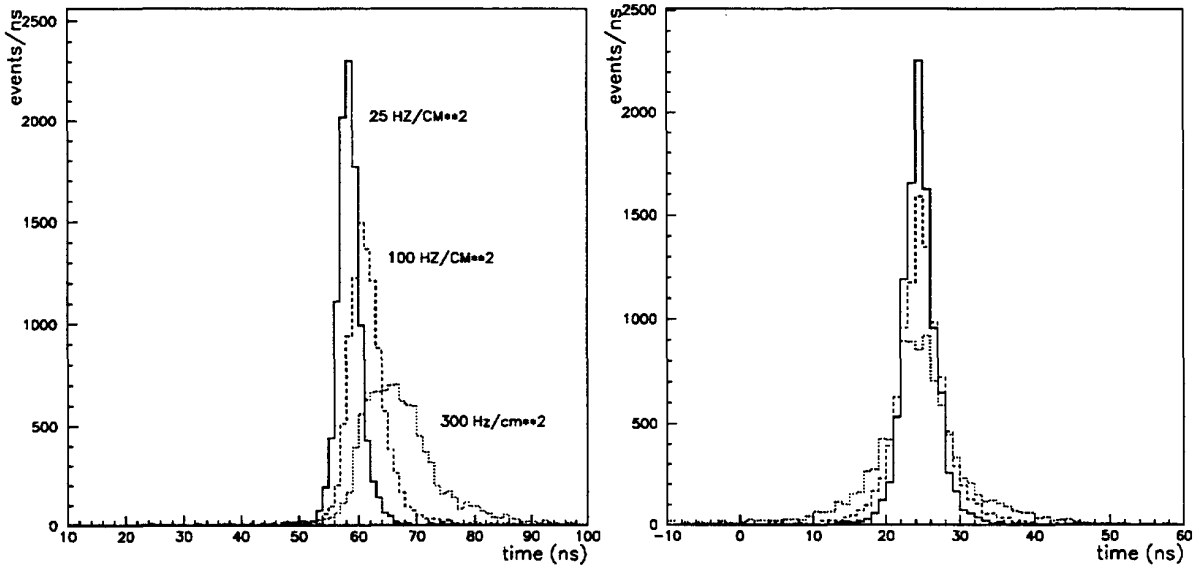

Figure 27: Distribution of the delay (a) relative to the trigger and (b) between two double-gap RPC for different particle fluxes: 25 Hz/cm^2 full line, 100 Hz/cm^2 dashed line, 300 Hz/cm^2 dotted line.

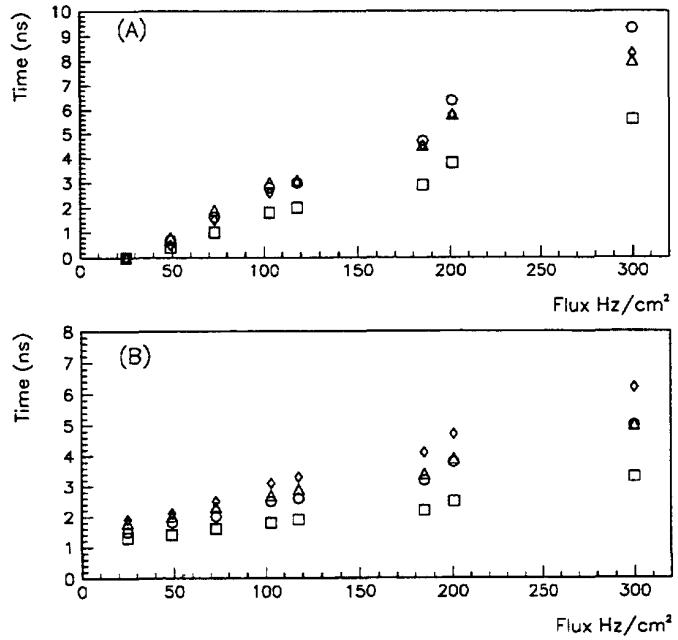

Figure 28: Delay (a) and time resolution (b) as a function of the particle flux for four RPCs: ○:Y9, □:Y10, △:Y11, ◇:Y12.

Fig. 27a shows the distribution of the delay for particle fluxes of 25, 100 and 300 Hz/cm^2. With increasing particle flux there is an increase of the average value due to slower response of the RPC at smaller values of the local electric field, and a broadening of the distribution can also be observed. We define *delay* as the average value of the distribution, and *resolution* as the r.m.s. width of a gaussian fit to the distribution. Referring to the data of Fig. 27a (chamber Y11), the

time distribution at 100 Hz/cm^2 has a small non-gaussian tail. The resolution is 2.7 ns and the time interval that contains 99% of the events is 20 ns. The distribution of the time difference between the two RPC in station 3 (chambers Y11 and Y12) is shown in Fig. 27b: the fraction of events with a coincidence within 25 ns is 1.00, 0.98, 0.92 for fluxes of 25, 100 and 300 Hz/cm ^{2} respectively. Fig. 28 shows the delay and the time resolution as a function of the particle flux for the four planes. The difference in performance reflects the different operation voltages chosen for the chambers. The best results, both in efficiency and time resolution, are obtained with chamber Y10 (the second double-gap RPC in station 2) which was operated at a voltage about 1000 V higher then the beginning of the efficiency plateau.

5.1.2 RPC operated at low gas gain

To operate a RPC with good efficiency and time performance at large particle fluxes we have followed two ways. Increase the conductivity of the electrode plates, thus reducing the recovery time of the detector, or reduce the amount of charge released in the discharge occurring in the gas. Though the first method has given positive results [6, 16], it has the disadvantage that the detector is more noisy and the power dissipated in the gas discharge is large. The second method implies to operate the detector at a low gas gain and to provide amplification with a front-end electronics that has a higher gain and, to preserve the good timing performance, high enough bandwidth [17]. A lower gas gain can be obtained either reducing the electric field or increasing the amount of quenching component in the gas mixture.

During the last RD5 runs we have measured the efficiency and the time resolution of an RPC operated at a lower gas gain. The measurements were done with a double-gap RPC of dimensions 0.5 x 0.5 m^2 with the read-out plane segmented in strips of 12 mm pitch. The eight central strips were equipped with a 150 MHz bandwidth amplifier. The pulses of the strips were divided by a passive splitter. Part was sent to a discriminator and a TDC and part read out in a charge integrating ADC. The RPC was operated with a gas mixture of argon-butane in the volume ratio 2:1 and containing different amount of freon from 4% to 80%. The local particle flux was defined as the ratio of the rate of the trigger counters and the beam profile measured with the proportional chambers and the silicon microstrip hodoscope.

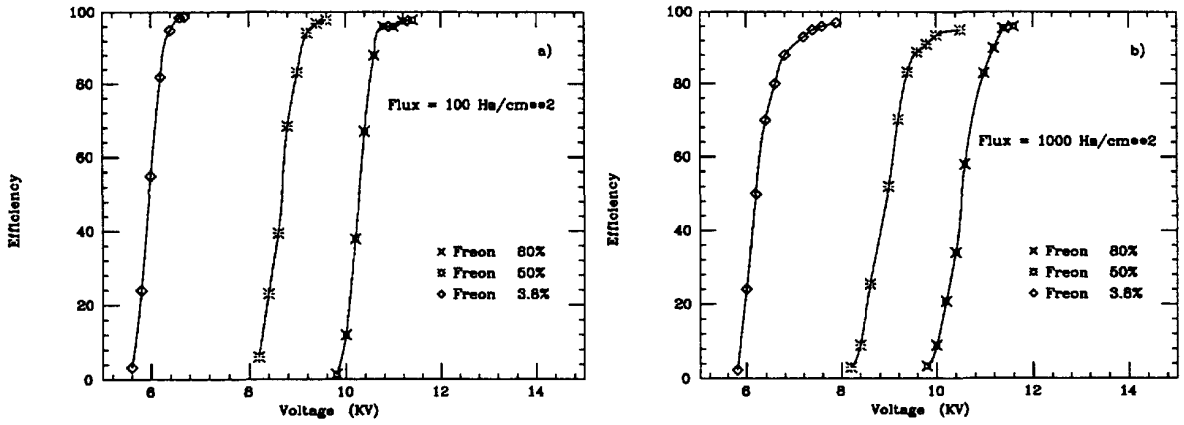

Figure 29: Efficiency as a function of the high voltage for different particle fluxes for an RPC operated at low gas gain.

Fig. 29 shows the efficiency as a function of the high voltage for different gas mixtures at a beam flux of $\approx$ 100 and 1000 Hz/cm^2. The behavior of the efficiency as a function of the particle flux is presented in Fig. 30. In this working mode RPCs show a clear improvement in the rate capability. Fig. 31a shows the time distributions of the RPC response measured at different beam fluxes. The gas mixture contained 80% of freon and the RPC operated at 11.8 kV. The distributions have very small non-gaussian tails. We quote as time resolution the width of a gaussian fit to the distribution. The time resolution is presented in Fig. 31b as function of the particle flux for the gas mixtures containing 4% and 80% of freon. A very good time resolution is achieved even at a flux of 3.9 kHz/cm^2 where the chamber is only 65% efficient.

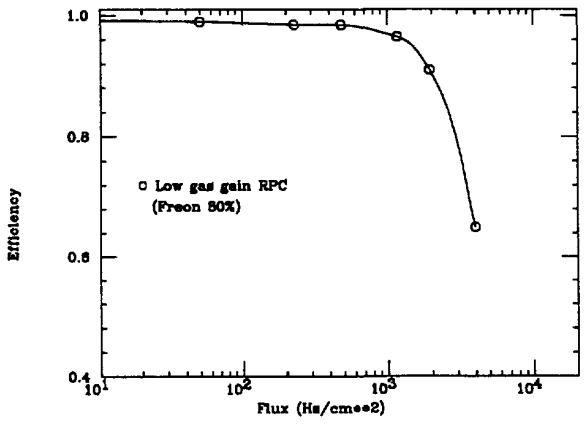

Figure 30: Efficiency as a function of the particle flux for an RPC operated at low gas gain.

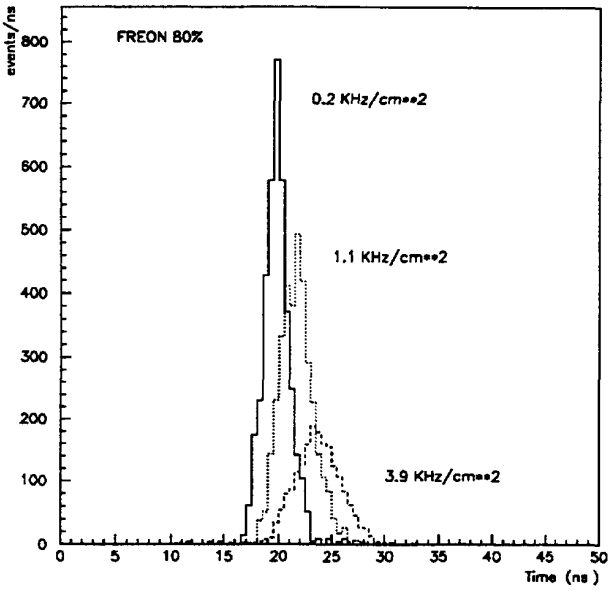

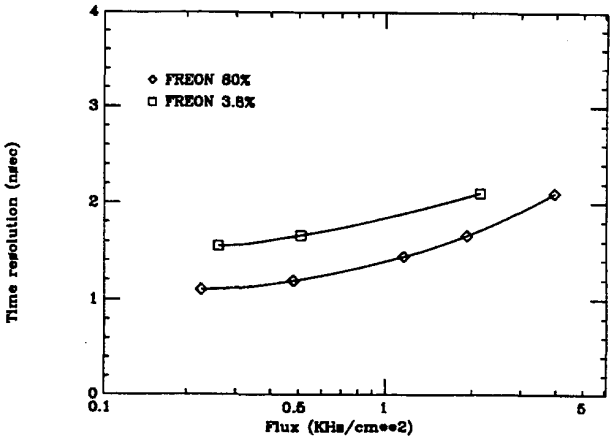

Figure 31: Distribution of the time response (a) and of the time resolution as a function of the particle flux (b) for an RPC operated at low gas gain.

5.1.3 Space resolution of RPC

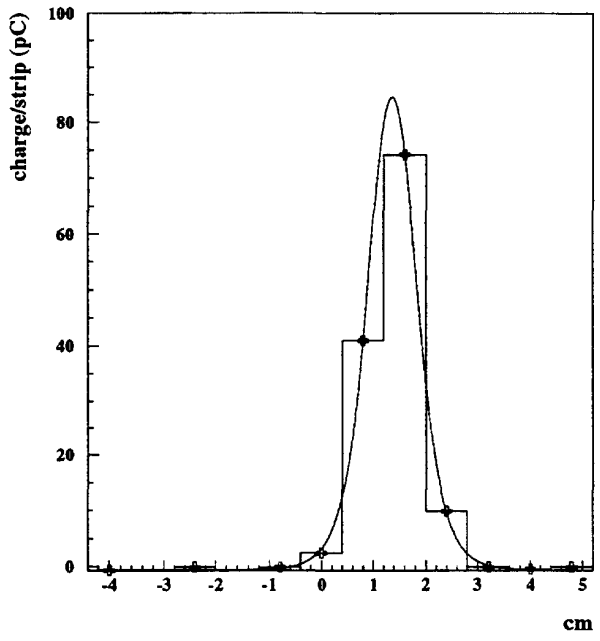

Figure 32: Charge induced on the RPC strips in one event.

A study of the space resolution of RPCs has been done with four single-gap RPCs of dimensions 0.5 × 0.5 m^2 with the read-out plane segmented in strips of 8 mm pitch. The RPCs were placed between the silicon microstrip hodoscope and the M1 magnet. The reconstruction of the position of the track was done reading the charge collected on the twelve central strips of each RPC and using the center of gravity method.

The strips were terminated on 50 Ω at one end while the other end was connected with a 50 Ω cable to a passive splitter, a ×10 voltage amplifier and a charge integrating ADC. The gate to the ADC was given by the trigger hodoscope and was shaped to be 75 ns long. The chambers were operated with a gas mixture of 58% argon, 38% butane and 4% freon and a voltage of 7.2 kV. The total charge collected on one end of the strips with minimum ionizing particles was ≈ 100 pC and the single strip noise was ≈ 0.1 pC. The calibration of the electronics was done by injecting a test charge at one end of the strips. Fig. 32 shows how the charge is distributed in one event. About 90% of the total charge is induced on three strips.

The position of the track was measured as the weighted average over three or five consecutive strips and compared with the extrapolation from the measurement in the silicon microstrip hodoscope. The distance between the two detectors is 70 cm and the error on the extrapolation is 30 μm. Fig. 33 shows for one RPC the correlation between the two measurements before applying any correction to account for systematics of the reconstruction method. The r.m.s. width of the residual distribution is ≈ 200 μm.

5.1.4 Warsaw RPC prototype

A prototype RPC chamber was constructed in Warsaw in spring '93. It was first tested with a radioactive iron source and with a cosmic ray telescope in Warsaw and subsequently brought to CERN for tests in the RD5 beam. We used the same gas composition as other RPCs: 58.2% Ar, 38.0% n-butane and 3.8% freon. The chamber size was 50×50 cm^2 and the strips were 1 cm wide. The plane specific resistivity was about 10^{12} Ω×cm. Twelve strips were read out with a LeCroy ADC. Their OR-ed signal was read with a TDC. Data were taken with various HV values and beam intensities.

In Figure 34a the chamber efficiency as a function of high voltage is shown for the incoming rate of about 10 Hz/cm^2. Figure 34b, shows the chamber efficiency versus incoming rate. The chamber behavior during the spill can be seen in the Figure 34c, which shows the efficiency as a function of time. For the rate of beam tracks of about 23 Hz/cm^2 the average

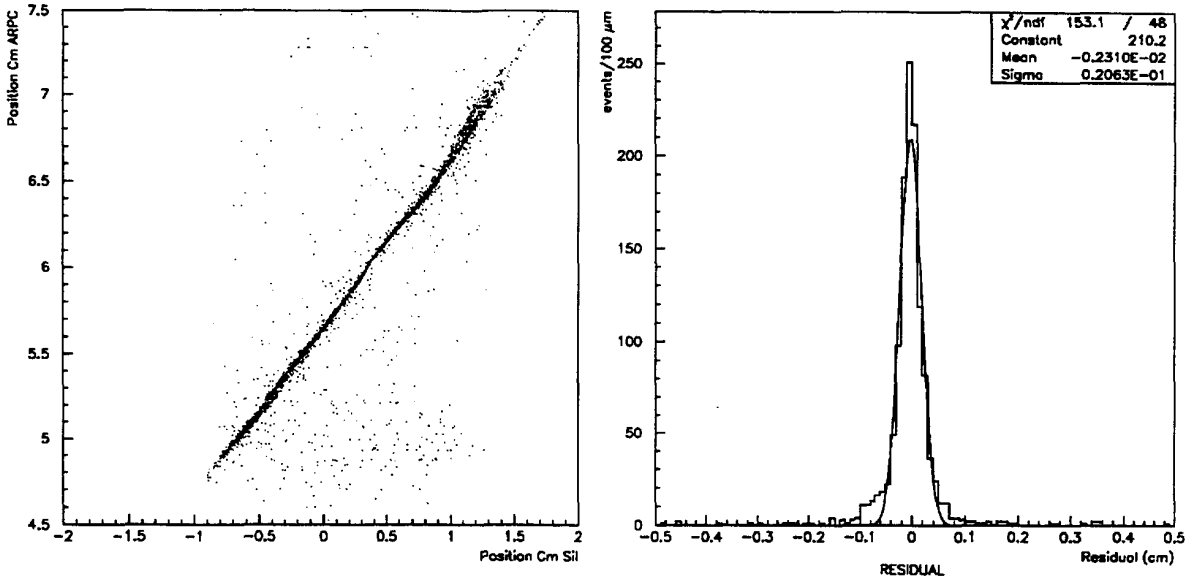

Figure 33: Correlation of the coordinate measured by the RPC with an analog readout and the silicon microstrip hodoscope (a) and distribution of the residuals before correction for systematics (b).

sum fell by 50% and the efficiency by about 20%. When the rate reached 370 Hz/cm^2 the efficiency drop was much more dramatic, it fell to about 10%. The TDC spectrum is shown in Fig. 34d. Its spread is about 7 ns. The average multiplicity of strips with ADC values above pedestal was about 3.5 corresponding to an avalanche size of 3.5 cm. The space resolution of the chamber was obtained by comparing the center of gravity of the ADC signals with the track position known from the beam reconstruction. The resolution was below 1 mm.

The chamber efficiency for high rates was not very good. In fact the Warsaw chamber plates were ordered and delivered with resistivity 10^{11} $\Omega\times$cm, but it rose up to 10^{12} $\Omega\times$cm during one month preceeding the tests in RD5. This fact points to the necessity of long term studies on material ageing.

A conclusion from these studies is that we understand better the operation of the RPCs, however, the chamber optimization process has to continue. First of all we would like to improve the chamber efficiency and the rate capability, minimize the response time uncertainty and reduce the cluster size.

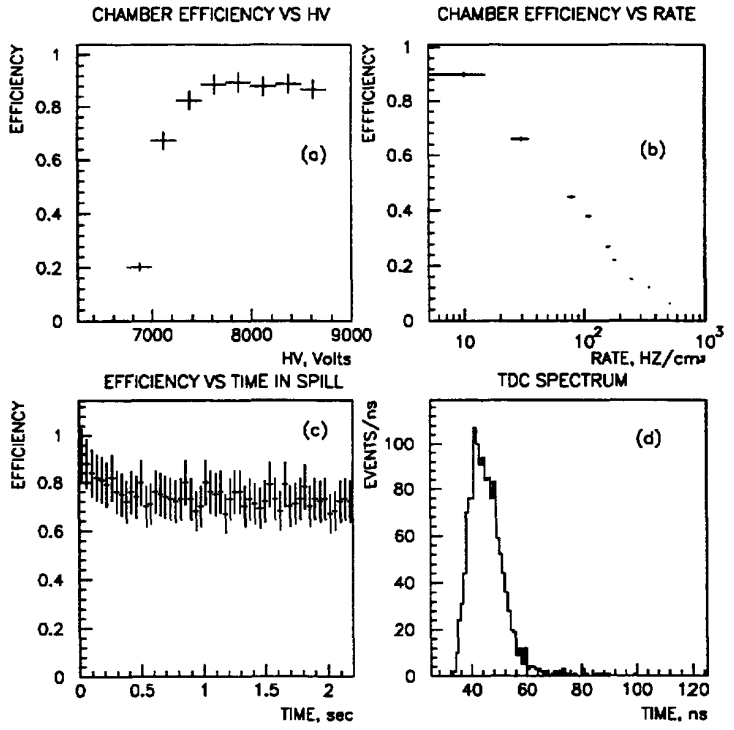

Figure 34: Results of Warsaw RPC prototypes tests in RD5

5.2 Parallel Plate Chambers (PPC)

A PPC chamber is a single gap gas detector with planar electrodes, working in avalanche mode [20]. The gap is very small (1-2 mm) leading to high electric fields. The chambers have a typical size of 5 × 5 cm^2.

A main feature in the chamber construction is the uniformity of the gas gap, both inside each PPC and between different PPCs. In fact, any variation in the gas gap would lead to differences in the electric field strength (and therefore in the gas gain) when applying the same high voltage.

In order to verify the gas gain uniformity over the entire PPC sensitive area we measured, for a given PPC, the detection efficiency as a function of the particle crossing point. All the efficiencies are equal within 3%, which is of the same order as the statistical error.

We also checked the gas gain uniformity over a sample of 26 PPCs coming from different deliveries from the same supplier (Guinchard SA, 1400 Yverdon-les-Bains, Switzerland), by irradiating each PPC with a ^{106}Ru radioactive source and measuring the average collected charge. We obtained a gas gain distribution with a sigma of 6.2%.

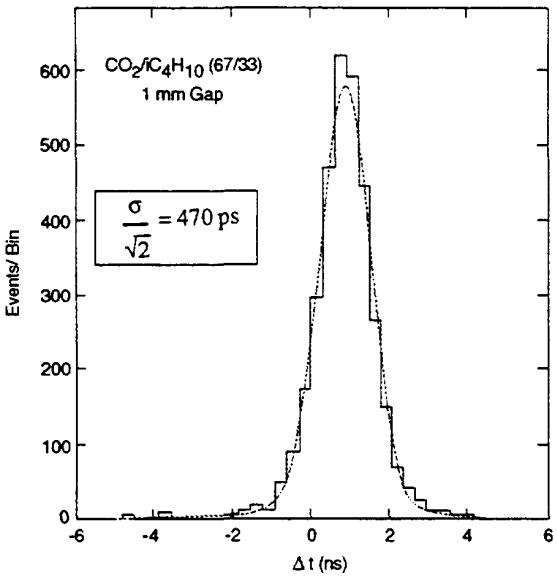

Figure 35: Time difference between two PPC's.

The time resolution has been measured for PPCs with different gas gaps (1 and 1.5 mm). Several gas mixtures of isobutane and carbon dioxide have been tested. The time resolution of the PPCs is practically independent of the gas mixture and chamber gap. The values obtained are about 500 ps (see Fig. 35).

Using the sum of signals from 2 PPCs we can reach a detection efficiency for minimum ionizing particles close to 100% for several gas mixtures (CO_2, CF_4 and CF_4/CO_2, CF_4/iC_4H_{10} and CO_2/iC_4H_{10} mixtures) with both 1 mm and 1.5 mm gas gaps. Within the experimental errors, no change of the detection efficiency has been observed for pion beams with intensities in the range 10^4 to 10^6 cm^{-2} s^{-1}. More intense beams are needed to pursue the test.

We have measured the stability of the response in terms of the efficiency as a function of time using a 2 × 2 cm^2 chamber. We observe variations smaller than 1% around the mean value during a one week period.

We have also constructed two prototype planes of ceramic PPCs. Each plane is an 8 × 8 PPC matrix mounted on a multilayer printed board. Analysis of results from a test in the RD5 test beam is in progress.

5.3 Fire Fly

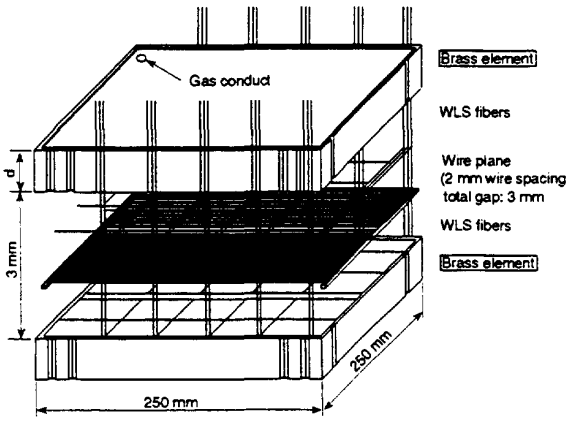

Figure 36: Structure of the Fire Fly chamber

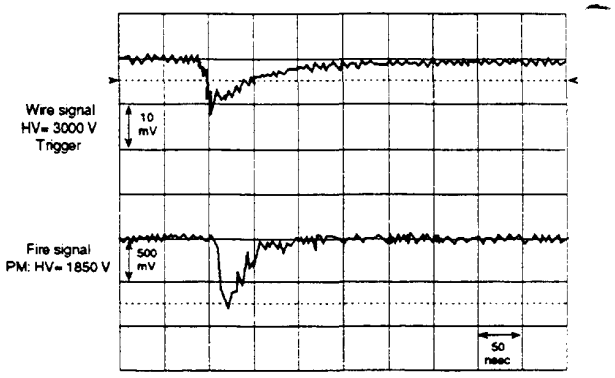

Figure 37: Scope picture of the wire and fiber signals

The FireFly chamber (see Fig. 36) is a thin gap (3 mm) chamber working eventually with pure CF_4 gas. A wire plane is inserted between two sintered brass plates which act as cathodes. The wires have a diameter of 50 μm and are spaced by 2 mm. Wavelength shifting fibers with a diameter of 1 mm are glued into grooves on the brass plate forming cells and they collect the light emitted by the avalanche at the wire when an ionizing particle crosses the chamber. A multianode phototube or another photosensitive device, far outside the detector, transforms this pulse into fast electric signal. The shape of the signal is shown in Fig. 37 compared to the signal from the wire.

A prototype of the Fire Fly chamber has been tested during the RD5 runs in 1993. A computer controlled recirculating gas system was used to keep the gas density constant. The analysis of the data is in progress. The first, preliminary results have shown a time jitter of the optical signal of 10 nsec with respect to the coincidence signal of the scintillators installed in front and on the back of the chamber.

5.4 Single Sided Stereo Silicon Detector

A single sided stereo angle detector (S3D) has been proposed as a simple, thin (in terms of radiation length) and relatively cheep device for LHC applications [22]. The layout of such a detector is shown in Fig. 38. The high resolution coordinate (called $r\varphi$) is measured by using the continuous strips aligned along the low resolution coordinate (called z). The inclined stereo strips are formed by connecting the short (3 mm) strips together. A typical charge deposition cluster in a detector will, on the average, fire a single $r\varphi$ and a single z-strip.

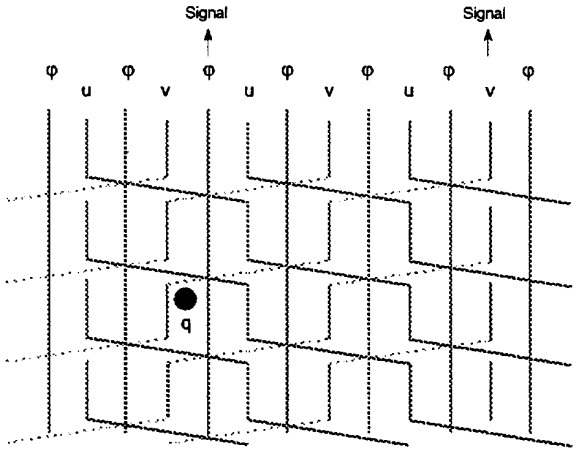

Figure 38: The layout of the single sided stereo angle detector

A S3D prototype has been tested in 1993. The SiBT was used to measure $r\varphi$ and z resolutions of the S3D detector at different angles of incidence of incoming particles from 0° to 30° in 5° steps. The distribution of the z-coordinate residuals is flat along the short strip (see Fig. 39) and does not depend significantly on the incident angle. Thus the accuracy of the z measurement does not exeed the short strip length i.e. ±1.5 mm. Measured $r\varphi$ residues at 10° are also shown in Fig. 39. The variances σ of the $r\varphi$ residual at different angles are shown in Table 6. This dependence could be expected as a similar behavior has already been reported for the n-side of the double sided detectors [23].

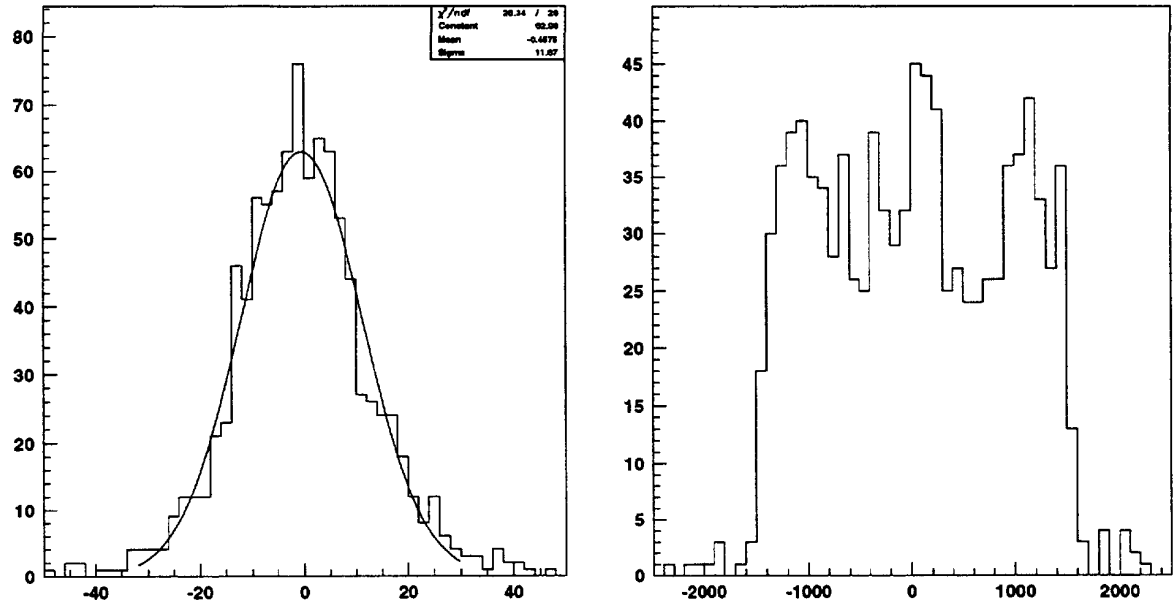

Figure 39: Residual in $r\varphi$ and z coordinate [μm]

Angle [degrees]	0	5	10	15	20	25	30
Variance σ [μm]	11	-	9	12	17	22	29

Table 6: Variances σ of $r\varphi$ residuals for various incident angles

5.5 Wall-Less Drift Chambers (WLDC) with Local Time Reference

A Wall-Less Drift Chamber (WLDC) [24] is a detector being desinged for the muon measurement at LHC. Severe timing conditions require a short drift time which is ensured by a small cell size (14 mm). This cell size also matches the granularity needed for the first level trigger. In order to avoid dead spaces walls between the cells are replaced by two cathode wires. An external time reference is given by RPCs coupled to the chamber.

A WLDC prototype consisting of 8 layers and 44 cells was tested to study its performance with a wide range of Ar/CO_2 gas mixtures of up to 80% CO_2 in a muon beam. The single cell detection efficiency is 99.9%. An example of single cell residuals is shown in Fig. 40 for 40% CO_2: at the working point of 2250 V it amounts to 165 μm. It turns out that for the range of 10% to 80% CO_2 the resolution fulfills the requirement for a 100 μm precise track segment in the bending plane, at each muon station. The μ-induced production of electromagnetic secondaries was also studied (see section 3.4).

These measurements were complemented by a test in a strong magnetic field of 3 Tesla nearly parallel to the direction of the muons and orthogonal to the chamber plane, as will be the case e.g. in the CMS forward muon stations. A reduced effective drift velocity and an increasingly non-linear space-time relationship (Fig. 41) are expected [25] at high magnetic fields.

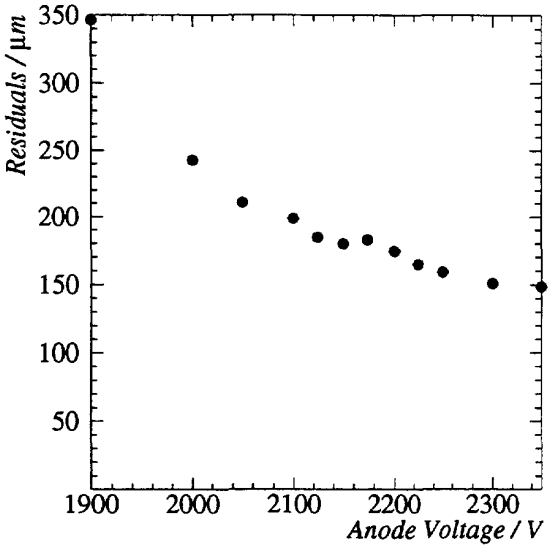

Figure 40: Residuals in the WLDC, for 8-point tracks and an Ar/CO_2 gas mixture of 60%/40%, as function of the anode voltage. The working point is 2250 V.

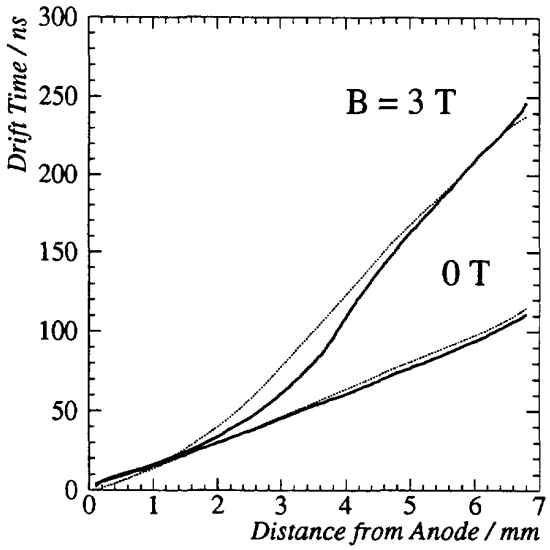

Figure 41: Space vs. time in the WLDC cell without and with a magnetic field of 3 T orthogonal to the chamber plane, from expectation (thin lines) and data (solid lines).

Since the superconducting magnet at RD5 does not feature the needed field orientation parallel to the beam, horizont cosmics in the desired direction were used as substitute. For these tests an Ar/CO_2 80%/20% gas mixture was used. The trigger was given by a coincidence signal from 3 RPCs, and the three individual times were also registered for offline checks and corrections. The timing requirement is more demanding in this application than later at the LHC, because here the RPC *alone* delivers the time reference for the drift chamber. A trigger time resolution of about 2.5 ns is deduced from the RPC data. The preliminary space-time relation obtained from the WLDC data, also included in Fig. 41, confirms the qualitative predictions of the simulation.

5.6 Drift Tubes with Bunch Crossing Identification (DTBX)

The DTBX is a new detector concept aiming to provide, using only one detector and one technique, the space resolution needed from a muon detector and the identification of the parent bunch crossing at the LHC: this goal was achieved working on a careful design of the drift cell and applying to the readout the mean-timer concept already described in Sec. 3.4.2.

The design is based on a plastic drift cell of 38 x 10 mm^2, whose side walls are coated with graphite paint to form a C-shaped cathode that provides a field shaping determining a rather linear space-time relationship in drift-velocity saturated mixtures. The tubes are superposed, staggered by half a tube, to form triplets or quartets of planes (see Fig. 12 and 13). The readout is done using a mean-timer-like logic circuit providing the drift time values at a fixed time after the muon crossed the cell.

In this scheme the space accuracy is determined by the time resolution of the mean-timer and the bunch crossing identification depends on the dispersion of the mean-timer output time.

Two prototypes were tested in the RD5 set-up using several gas mixtures: Ar(70%)/iso-C_4H_{10}(30%), Ar(40%)/C_2H_6(60%), Ar(88%)/CO_2(12%), Ar(85%)/CO_2(15%) and Ar(82%)/CO_2(18%). In all mixtures the prototypes reached an operating efficiency of 97%. The readout was done using both available analog mean-timers and TDCs. The space resolution obtained was ranging from 150 μm to 200 μm per cell and the timing resolution for bunch crossing identification given from the mean-timer method was of $\simeq$ 3 ns for tracks inclined up to 20 degrees. The time resolution is shown in Fig. 14 for tracks normal to the chamber. It is clear that the method fails to identify bunch crossing in presence of backgrounds due to δ-rays production off the cell walls and muon bremsstrahlung. A study of the response of the DTBX chamber to muons accompanied by additional particles originating from electromagnetic showers is presented in section 3.4.

5.7 GEM Cathode Strip Chambers (CSC)

The CSC is a multiwire proportional chamber with segmented cathode readout. They can provide precision in the bend coordinate by interpolation, in the non-bend coordinate by anode wires, and provide trigger and timing. The entire (central and forward) GEM muon spectrometer [26] is based on this technology,

Two CSC prototypes have been tested in 1992 and 1993 runs. These prototypes were built as two-gap modules. The two gaps were formed by three flat, rigid panels made of a sheet of nomex honeycomb and two copper-clad FR4 laminates, which formed the cathodes of the two proportional chambers. The panel frames were made of machined zelux (fiberglass reinforced lexan). They provided the 2.5 mm step for the anode plane of gold-plated tungsten wires 30 μm in diameter with a 2.5 mm pitch. The frames of the outer panels had a milled cavity with enough room for the epoxy beads for the wire attachment as well as the anode blocking capacitors. A rubber gasket just outside this cavity provided the gas seal for the assembly. The position sensing cathode strips were etched with a 5mm readout pitch. These cathodes were precisely positioned with respect to each other with the aid of locating pins. The strips were oriented at 90 degrees with respect to the anode wires providing the precision position measurement in a direction along the wires.

Tests during the 1993 RD5 running were conducted using the 0.5 x 0.5 m^2 four layer chamber assembled at BNL. Significant improvements in the cathode readout electronics allowed us to get substantial improvements in resolution over that obtained in the 1992 runs [27] The main improvements were the inclusion of a preamplifier in front of the amplex chip [28] to better match the capacitive load of the strips and a better calibration scheme.

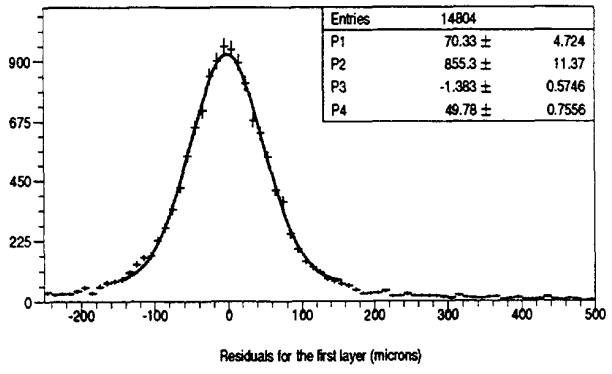

Figure 42: CSC single layer spatial resolution – the residuals of first layer relative to a line fit to the other 3 layers.

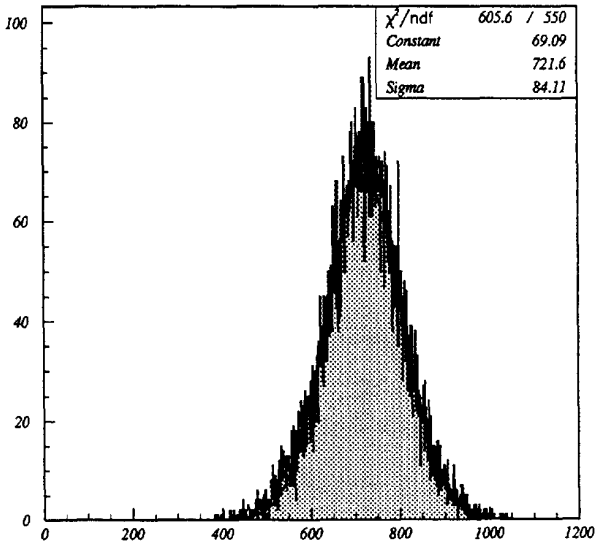

Figure 43: Arrival time distribution (50 ps bins) of the logical OR of all 4 layers of the CSC.

Preliminary results indicate a single layer spatial resolution of 50 μm. This is shown in Fig. 42, where the residuals of the first layer relative to a line fit to the other 3 layers is plotted. Both the FWHM/2.35 and the fit to the distributions of a constant plus gaussian in the $\pm 3\sigma$ range (shown on the plot) give 50 μm as the chamber resolution. All four layers demonstrate the same resolution.

One of the main functions of the GEM muon system is to provide a beam crossing tag. This will be provided by the anode readout. Preliminary timing results are shown in Fig. 43 which shows the earliest arrival time distribution provided by the logical OR of all four layers of the chamber. The actual anode readout electronics is a design using conventional discriminators which are known to have pulse height slewing effects. Despite this, the 4.2 ns resolution shown in Fig. 43 almost meets the GEM muon system requirement of tagging the beam crossing with > 99% efficiency (recall this is for a 6 layer superlayer, not 4).

Other studies using these data include: single layer resolution as a function of incident angles (polar and azimuthal) [29] and resolution as a function of gas gain. We also have data with different materials directly in front of the chamber: 40 cm of copper and 40 cm of iron. This will allow us to study effects such as muon-induced showers, which are important

to the first chamber directly behind the calorimeter. In addition we have data with multiple tracks to study two track resolution.

In the 1993 September-October run a similar CSC built in Dubna (see Sec. 7) was successfully tested in various magnetic field configurations and without magnetic field. Analysis of data is in progress.

5.8 Honeycomb Strip Chambers (HSC)

The Honeycomb Strip Chambers (HSC) [14] are high performing muon chambers which can be produced in a large number at low cost for LHC experiments. The HSC is a two-coordinate position sensitive detector. The coordinates of a track are determined by cathode readout of the strips and drift time measurement by the anode wires.

Single-layer HSCs being part of TRACAL and two types of multilayer HSC have been tested in RD5 since 1992. The characteristics of a small 0.3×0.3 m^2 8 layer prototype (P1) were measured under various conditions in the RD5 muon beam. Three large 3.25×1.00 m^2 prototypes (P2s) were constructed at NIKHEF. The individual properties of the chambers were measured and the concept of projective alignment is studied. Preliminary results are given for the measured error on the sagitta.

5.8.1 Single layer HSCs in TRACAL

The single layer HSCs in TRACAL were tested with several gas mixtures. The behaviour of the efficiency as a function of the applied high voltage on the anode wire is shown in Figure 44 for an Ar/CO_2 70/30 mixture. The three efficiency curves correspond to three discriminator thresholds. The data were taken with 200 GeV/c muons. The beam chambers were used for normalisation purposes. The efficiency plateau appears approximately at 87 % which corresponds to the geometrical coverage of a single layer honeycomb structure.

Resolution studies for both strip and wire coordinates are in progress. These studies, in addition to the general behaviour of single layer HSCs, will also be performed using muon data which are taken at several magnetic field strengths.

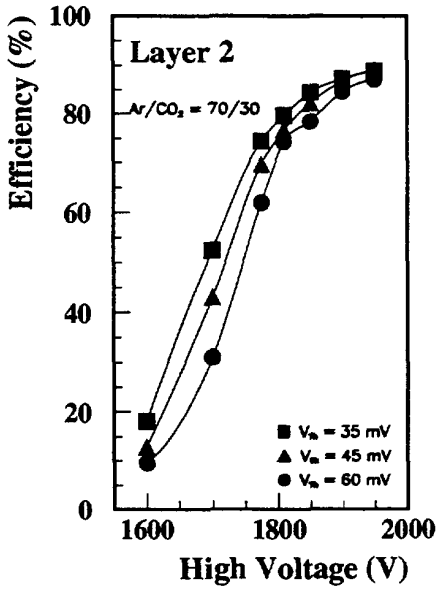

Figure 44: The efficiency of a single layer HSC as a function of HV for three discriminator thresholds.

5.8.2 The P1 chamber

The P1 HSC is an 8 layer superlayer. Each layer consists of 54 strips and 32 wires and is similar to the monolayers used in TRACAL. By gluing the layers together a self supporting rigid structure is created. During the tests in RD5, the behavior of the HSC as a drift-tube was the main interest.

Three types of studies were performed. First of all, the spatial resolution was measured for different gases, high voltages and incoming angles φ and θ. Next, the chamber was positioned behind 1.2 m of iron to study the EM-shower contamination for different muon momenta. Finally, the chamber was tested in the 3 T M1 magnet. The chamber was oriented such that the field lines were parallel to the wires and perpendicular to the strips. Because of the Lorenz angle, the drift distance versus drift time relation $(r - t)$ is dependent on the magnetic field and the drift gas.

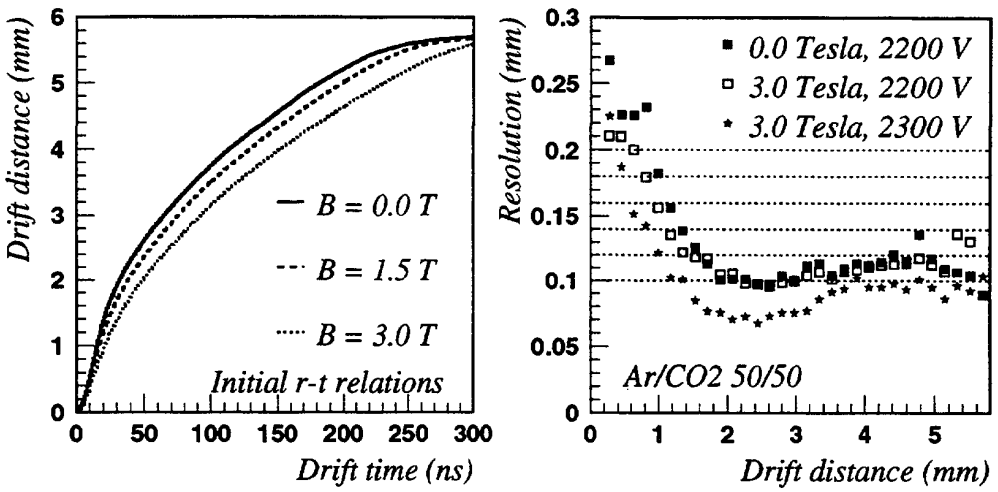

Figure 45: HSC P1 test results: a) The $r - t$ relations for 3 different fields for an Ar/CO_2 50/50 mixture, b) Spatial resolution for B=0T and B=3T. For B=3T the numbers are given for HV = 2200V and HV = 2300 V.

The $r - t$ relation for 3 different magnetic field strengths for an Ar/CO_2 50/50 mixture are given in Figure 45a. The spatial resolution curves for different magnetic fields. are shown in Figure 45b. The resolution close to the wire ($r = 0$) is limited by primary ionization statistics. One can see that in homogeneous fields there is no negative effect on the performance of the chamber for fields up to 3 T. The average resolution is approximately 130 μm/layer. A better resolution was obtained with a higher high voltage, unfortunately this data was only taken for the 3 T field.

5.8.3 The P2 chambers

The three P2 chambers were tested at RD5 in 1993. Each P2 chamber consists of 8 active layers with 192 strips and 256 wires each. Only 16 wires of each layer and a variable number of strips were read out. The most upstream chamber was positioned 0.3 m behind 1.2 m of iron to generate EM-showers. A VME Transputer system was used for the readout of the strips and wires. A stand alone readout was created with a transputer link to the RD5 data aquisition system.

Six CCD/RASNIK alignment systems were installed [21] on the chambers.

The analysis is still in progress, but a preliminary result for the spatial resolution of the strips less than 85 μm can be reported. The spatial resolution measured with the wires depends on the type of electronics used. Under experimental conditions similar to the P1 tests, the behavior is equal to that of the small prototype. By combining the data of the 3 individual chambers a sagitta ϵ can be measured ($\epsilon = Z_2 - \frac{1}{2}(Z_1 + Z_3)$, with $Z_{1,2,3}$ being the coordinates measured with the wires). The preliminary measured error in ϵ is 93 μm, but the search for systematics has not been finished yet.

6 Conclusions and Plans for 1994

The main results achieved by the RD5 collaboration can be summarized as follows:

- Considerable improvement of many parts of the detector has been made.
- All the data taking required by the physics program is completed.
- Analysis of the total punchthrough is near to finish.
- Analysis of the momentum and angular spectrum of punchthrough is in progress, the first results are available.
- The simulation program of the RD5 setup is ready and the first comparisons of the simulated and measured data have been made.
- The study of muon induced electromagnetic secondaries based on measurements by different chambers is in progress.
- Three different trigger processors based on RPCs have been tested.
- Protoypes of various kinds of chambers aimed to be used for muon triggering (RPC, PPC, FireFly) or tracking (HSC, CSC, DTBX, WLDC) have been extensively studied.

In 1994 we would like to continue the chamber test program including tests of large scale prototypes:

- A large size DTBX will be installed in the muon station 3.
- A large (about 1 m^2) WLDC with 10-layer aluminium structure and two smaller prototypes, one with cells made of a conductive PVC and the second one made of a rigid foam coated with conductive paint will be tested.
- A HSC having 5.7 m long anode wires and different cell size will be tested in M1.
- Two types of CSC will also be tested in the magnetic field parallel and perpendicular to the drift direction.
- Tests of RPCs with low gas gain will be continued with different gas mixtures and at various beam conditions, especially with high flux illuminating a large area of the chamber.
- A new Warsaw RPC, PPCs, and FireFly chamber will also be tested.

An extensive program of tests of different trigger processors which started in 1993 will also be continued in the next year.

To continue the RD5 program we request for 1994 four weeks of beam time dedicated to RD5. We also request an amount of 200 kCHF from CERN to cover part of the running costs which include magnet operation, the gas supplies, POOL electronics, new readout electronics, tapes, some modifications in the experimental area etc.

7 New Collaborators and Responsability Breakdown

Since the previous Status Report the following institutes joined the RD5 collaboration:

In 1992:

C. Albajar
Universitad Autonoma, Madrid, Spain

P. Le Coultre
ETH, Zurich, Switzerland

After the 1993 run period:

I. Golutvin, V. Karjavin, Yu. Kiriushin, P. Moissenz, S. Movchan,
S. Selunin, S. Sergueev, N. Zamiatin and A. Zaroubin
Joint Institute fir Nuclear Research (JINR), Dubna, Russia

Responsibilities of members of the RD5 Collaboration are listed in Table 7

Institute	Responsability
Aachen	muon drift chambers, WLDC, physics analysis
Amsterdam	TRACAL, HSC
Boston	GEM CSC
Brookhaven	GEM CSC
Budapest	RD5 running, PPC
CERN	RD5 running, physics analysis
Dubna	Dubna CSC
Firenze	PPC
Helsinki-SEFT	SiBT, physics analysis
Helsinki-LabHEP	physics analysis
Louisiana	simulation
Madrid-CIEMAT	PPC
Madrid-Univ.	physics analysis
Moscow	PPC
Nijmegen	TRACAL, physics analysis
Padova	DTBX, electronics for TRACAL, physics analysis
Roma-La Sapienza	RPCs, Coinc. M. Trig. Proc., physics analysis
Roma-Tor Vergata	RPCs, WRM Trig. Proc., physics analysis
Stony Brook	simulation, GEM CSC
Turku	SiBT
UCLA	muon drift chambers, Dubna CSC, physics analysis
UC-Riverside	muon drift chambers, Dubna CSC
Vienna	DAS, RD5 running
Warsaw	RPC, PACT Proc., physics analysis
Zurich	FireFly

Table 7: Breakdown of responsabilities

References

[1] M. Della Negra et al., *Study of Muon Triggers and Momentum Reconstruction in a Strong Magnetic Field for a Muon Detector at LHC*, CERN/DRDC/90-36, DRDC/P7.

[2] A. Böhrer et al., *Status Report of the RD5 Experiment*, CERN/DRDC/91-53.

[3] M. Aalste et al., Z. Phys. C **60** (1993) 1-10.

[4] F. Bakker et al., Nucl. Instr. and Meth. in Phys. Res. **A330** (1993) 44.

[5] F. Gasparini et al., Nucl. Inst. and Meth. in Phys. Res. **A 336** (1993) 91.

[6] M.Andlinger et al. (RD5 Collaboration), *Study of Resistive Plate Chambers for muon detection at hadron colliders*, Internal Note 1015, Dipartimento di Fisica Università di Roma La Sapienza, 9.7.1993, to be published in Nuclear Instruments and Methods in Physics Research.

[7] A. Arefiev et al., *A measurement of the First Townsend coefficient in CF_4, CO_2 and CF_4/CO_2 mixtures at high, uniform electric field*, CERN-PPE/93-82, 5 April 1993, to be published in Nucl. Instr. and Meth. in Phys. Res. A

[8] M. Aguilar-Benitez et al., Nucl. Instr. and Meth. in Phys. Res. **A258** (1987) 26.

[9] Private communication from NA36 experiment.

[10] J. L. Bénichou, A. Hervé. G. Waurick, *Absorber magnet for RD5 (AM)*, RD5 technical note RD5 TN/91/01.

[11] G. Wrochna, *RD5 Trigger System '93*, RD5 technical note RD5 TN/93-14.

[12] R. Brun et al., GEANT User's Guide, CERN DD/EE/83.

[13] C. Lyndon et al., RD5 technical note RD5 TN/93-13.

[14] H. van der Graaf et al., Nucl. Instr. and Meth. in Phys. Res. **A307** (1991) 220.

[15] H. Czyrkowski et al., *RPC Based CMS Muon Trigger*, CMS TN/93-111.

[16] L.Pontecorvo (RD5 Collaboration):*Study of the characteristics of Resistive Plate Chambers in the RD5 experiment*, proceedings of the International Workshop on Resistive Plate Chambers in Particle Physiscs and Astrophysics, ed. G.Ciapetti, S.Ratti, R.Santonico, Scientifica Acta **8** (1993) 145.

[17] R.Cardarelli, A.DiCiaccio and R.Santonico: Nuclear Instruments and Methods in Physics Research, **A333** (1993) 399.

[18] E.Petrolo and S.Veneziano: *Use of GaAs circuits for first level muon triggering at LHC*, presented at the 5th Topical Seminar on Experimental Apparatus for High Energy Particle Physics and Astrophysics, San Miniato, Italy, 26-30 April 1993.

[19] R. Cardarelli et al. Nucl. Instr.and Meth. in Phys. Res. **A324** (1993) 253-259.

[20] A. Arefiev, *Construction and performance of Parallel Plate Chamber prototypes*, RD5 TN/92-04.

[21] H. Dekker et.at.: The RASNIK/CCD 3-dimensional alignment system. Proceedings of the 3rd Conference of Accelerator Alignment, CERN/Annecy, Oct. 1993. Page 147.

[22] M. Huhtinen at al., *Single Sided Stereo Angle Silicon Strip Detector*, IEEE Nuclear Science Symposium, Orlando, November 1992, to be published in NIM.

[23] R. Brenner et al., *Measurement of Spatial Resolution of Double-sided Double-metal AC-coupled Silicon Microstrip Detectors*, Sixth European Symposium on Semiconductor Detectors, Milano, Italy, February 24-26, 1992.

[24] H. Faissner et al., Nucl. Instr. and Meth. **A330** (1993) 76.

[25] We used the programs WIRCHA by J. Fehlmann, J. Paradiso and G. Viertel (ETH Zürich/IHP, 1983), and GARFIELD by R. Veenhof, CERN program library.

[26] GEM Collaboration, *GEM Technical Design Report*;
GEM technical note TN-93-262 (1993).

[27] J. Shank et al., *Test beam results from the GEM Prototype CSC in RD5*, GEM technical note TN-93-402 (1993).

[28] E. Beuville, et al., *Amplex – A Low noise, low power Analog CMOS Signal Processor for Multi-element Silicon Particle Detectors*, CERN/EF89-9 (1989).

[29] V. A. Polychronakos and V. Tcherniatine, *The effect of Inclined tracks and the Lorentz angle in the Spatial Resolution of the Interpolating Cathode Strip Chambers*, GEM technical note TN-92-137 (1992).